Journal of Experimental Botany, Vol. 76, No. 4 pp. 1049–1067, 2025
https://doi.org/10.1093/jxb/erae466 Advance Access Publication 19 January 2025

RESEARCH PAPER

The *PEBP* genes *FLOWERING LOCUS T* and *TERMINAL FLOWER 1* modulate seed dormancy and size

Judit Nadal Bigas[1,2], Martijn Fiers[2], Froukje van der Wal[2], Leo A.J. Willems[3], Viola Willemsen[4], Harm Nijveen[5], Gerco C. Angenent[1,2], and Richard G.H. Immink[1,2,*]

[1] Laboratory of Molecular Biology, Wageningen University and Research, 6708PB, Wageningen, The Netherlands
[2] Bioscience, Wageningen Plant Research, Wageningen University and Research, 6708PB, Wageningen, The Netherlands
[3] Laboratory of Plant Physiology, Wageningen University, 6708PB Wageningen, The Netherlands
[4] Laboratory of Cell and Developmental Biology, Wageningen University and Research, 6708PB Wageningen, The Netherlands
[5] Bioinformatics Group, Wageningen University and Research, 6708PB Wageningen, The Netherlands

* Correspondence: richard.immink@wur.nl

Received 22 August 2024; Editorial decision 12 November 2024; Accepted 17 January 2025

Editor: Scott Boden, University of Adelaide, Australia

Abstract

The phosphatidylethanolamine-binding protein (PEBP) family members FLOWERING LOCUS T (FT) and TERMINAL FLOWER1 (TFL1) are major regulators of plant reproduction. In Arabidopsis, the FT/TFL1 balance defines the timing of floral transition and the determination of inflorescence meristem identity. However, emerging studies have elucidated a plethora of previously unknown functions for these genes in various physiological processes. Here, we characterized potential roles in seed size and dormancy of *FT* and *TFL1* in *Arabidopsis thaliana* using CRISPR mutants and reporter analysis. Our findings unveiled a role for *TFL1* in seed dormancy while confirming the role of *FT* in regulating this trait. We showed that the interplay between these two genes in seed dormancy is antagonistic, mirroring their roles in flowering time and inflorescence architecture. Analysis of reporter lines demonstrated that *FT* and *TFL1* are partly co-expressed in seeds. Finally, we showed that total seed yield is affected in these mutants. Together, our results highlight the versatility of these two genes beyond their canonical functions. The impact of *FT* and *TFL1* on seed characteristics emphasizes the significance of approaching gene studies from various perspectives, enabling the identification of multifaceted molecular factors that could play a major role in shaping the future of agriculture.

Keywords: *Arabidopsis thaliana*, *FLOWERING LOCUS T* (*FT*), flowering time, *PHOSPHATIDYLETHANOLAMINE-BINDING PROTEIN* (*PEBP*), seed dormancy, seed size, seed yield, *TERMINAL FLOWER 1* (*TFL1*).

Introduction

Successful plant reproduction is an essential element for the survival and evolution of plant species. In flowering plants, it hinges upon the precise coordination of various individual processes that lead to the formation of seeds, the ultimate product of reproduction. The reproductive journey encompasses multiple stages, including floral transition, development of floral organs, fertilization, seed formation, seed maturation, and, eventually, seed germination. Complex gene regulatory networks govern these intricate processes, with multiple interconnected pathways at play. Extensive studies have identified and characterized

several genes within these pathways (Jack, 2004; Robles and Pelaz, 2005; Benlloch *et al.*, 2007; Holdsworth *et al.*, 2008; Leijten *et al.*, 2018; Zhou and Dresselhaus, 2019; Verma *et al.*, 2022). Among the central players are *FLOWERING LOCUST* (*FT*) and *TERMINAL FLOWER1* (*TFL1*) (Chen *et al.*, 2014; Wickland and Hanzawa, 2015; Zhang *et al.*, 2020; Wang *et al.*, 2022). These genes belong to the phosphatidylethanolamine-binding protein (PEBP) family, which is known for its signaling functions in bacteria, animals, and plants (Wickland and Hanzawa, 2015). Both *FT* and *TFL1* encode small globular proteins and share a significant degree of amino acid sequence identity (Ahn *et al.*, 2006). Research conducted across different plant species has demonstrated the universal and versatile involvement of these two genes throughout the entire reproduction process.

In the early phase of the reproductive process, commonly known as the floral transition, *FT* and *TFL1* play crucial yet opposing roles (Ahn *et al.*, 2006). In *Arabidopsis thaliana*, the FT protein promotes the switch from vegetative to reproductive development, ultimately leading to flowering (Koornneef *et al.*, 1998; Kardailsky *et al.*, 1999; Kobayashi *et al.*, 1999). Conversely, the TFL1 protein suppresses this transition by maintaining the meristem in a vegetative state (Shannon and Meeks-Wagner, 1991; Bradley *et al.*, 1997). During this phase, *FT* is specifically expressed in the leaf vascular tissue, and its protein is transported to the shoot apical meristem (SAM) through the phloem, acting as a systemic flowering inducer (Corbesier *et al.*, 2007; Mathieu *et al.*, 2007). In contrast, TFL1 functions locally within the SAM meristem, with its expression being limited to the central meristematic regions and its protein being able to move to the outer layer (Conti and Bradley, 2007; Goretti *et al.*, 2020).

In addition to their functions in flowering time control, *FT* and *TFL1* also play a role in determining inflorescence structure and overall plant architecture in an opposing manner. *FT* primarily promotes the transition from indeterminate to determinate plant growth, while *TFL1* is involved in the maintenance of the shoot apex, allowing for indeterminate growth of the inflorescence (Alvarez *et al.*, 1992; Conti and Bradley, 2007). As a result, in *ft* mutants, there is an increase in vegetative growth, and the apical and axillary meristems give rise to indeterminate shoots, whereas in *tfl1* mutants vegetative growth is minimized and primary and secondary inflorescences are converted into a terminal flower meristem (Bradley *et al.*, 1997; Moraes *et al.*, 2019; Liu *et al.*, 2021).

Nonetheless, the *FT*/*TFL1* gene family encompasses various functions associated with reproduction that extend beyond the regulation of flowering time and inflorescence architecture. In the Arabidopsis Landsberg *erecta* (L*er*) background, *FT* has been suggested to play a role in transgenerational memory, in which the mother plant influences the germination of offspring seeds (Chen *et al.*, 2014; Chen and Penfield, 2018). The study provides evidence that *FT* expression in fruit tissues suppresses proanthocyaninidin biosynthesis and modifies the tannin content of seed coats. Consequently, both these processes exert an influence on the final dormancy level of progeny seeds (Chen *et al.*, 2014). In addition to that, more recently, *TFL1* has emerged as a key regulator of seed development. Mutations in the Arabidopsis Columbia (Col) *TFL1* gene result in larger seeds without altering the seed number per silique (Zhang *et al.*, 2020). This effect on seed size is attributed to a delay in the time of endosperm cellularization. Intriguingly, *TFL1* is expressed in the chalazal endosperm, while its protein predominantly localizes within the peripheral endosperm. This observation raises the possibility that the TFL1 protein might exhibit movement within the seed, similar to what has been demonstrated in the SAM (Conti and Bradley, 2007; Zhang *et al.*, 2020).

Over the past few years, there has been an increasing interest in exploring the involvement of *FT* and *TFL1* genes in traits associated with seed development. These analyses have also extended across multiple species. Notably, an *Oryza sativa TFL1* homolog, *CENTRORADIALIS 2* (*OsCEN2*, also known as rice *TFL1*/*CEN* homolog, *RCN1*), has been proposed to act as a negative regulator of grain size. Overexpression of *OsCEN2* in rice reduces grain size, while its knockout produces larger, heavier grains (He *et al.*, 2022). In *Solanum lycopersicum*, transgenic plants overexpressing *SELF PRUNING 3C* (*SP3C*), a tomato *TFL1-like* member, exhibit delayed germination when compared with a wild-type tomato (dos Reis Moreira *et al.*, 2022). Likewise, in Moso bamboo (*Phyllostachys heterocycla*), the *PhFT1 TFL1-like* member has been identified for its significant expression in both flowers and seeds, and its ability to inhibit the rate of seed germination (Yang *et al.*, 2019).

The roles of *FT*/*TFL1* genes are of utmost importance in determining the vitality and successful development of both flowers and seeds. Consequently, they make a significant contribution to the evolutionary fitness and the overall crop yield in flowering plants. Despite numerous studies focusing on the seed-related functions of these two genes, their comprehensive roles in this tissue remain far from being fully understood. So far, *FT* has been recognized as a significant contributor to the regulation of seed dormancy, a state in which seeds are prevented from germinating even in the presence of favorable conditions (Chen *et al.*, 2014, 2021). Similarly, TFL1 has been identified as a pivotal factor in controlling seed size (Zhang *et al.*, 2020). Nevertheless, there are still many unanswered questions regarding their precise mechanisms of action, their interactions with other genetic and environmental factors, and their potential involvement in other essential seed characteristics. In the present study, we have characterized unexplored seed functions of Arabidopsis *FT* and *TFL1* by creating single and double mutants using CRISPR/Cas9 [clustered regularly interspaced palindromic repeats (CRISPR)/CRISPR-associated protein 9] genome editing. The *tfl1* mutants exhibited reduced seed dormancy, whereas the loss-of-function mutant of *FT* displayed minimal to negligible variation in seed size. Additionally, we have

observed that *FT* and *TFL1* show co-localization in maternal regions, but only *TFL1* is found within the endosperm tissue of fertilized seeds. Our findings reveal *TFL1* as a novel regulator of seed dormancy in Arabidopsis (L*er*). Additionally, we shed light on the interactions between *FT* and *TFL1* in the control of seed quality characteristics and the possible molecular execution of these functions in concert with A-class bZIP transcription factors.

Materials and methods

Plant materials and growth conditions

Arabidopsis thaliana accession L*er* was used as the wild-type control, serving as the background for all genetic modifications conducted. The selection of the Arabidopsis accession is based on the previously documented dormancy characteristics of the L*er* ecotype (Koornneef *et al.*, 2000). Three independent *ft* mutant lines (*ft-cr1*, *ft-cr2*, and *ft-cr3*), three independent *tfl1* mutant lines (*tfl1-cr1*, *tfl1-cr2*, and *tfl1-cr3*), and two independent *bzip67* mutant lines (*bzip67-cr1* and *bzip67-cr2*) were obtained via CRISPR/Cas9-based mutagenesis and *Agrobacterium tumefaciens*-mediated transformation. Homozygous mutant lines lacking the transgene were selected and utilized for subsequent analyses. The *ft-1* mutant was obtained from the European Arabidopsis Stock Centre (NASC: CS56).

Wild-type Arabidopsis L*er*, single and double *ft tfl1* mutants, and *bzip67* mutant S_3 (third generation by self-fertilization) seeds were stratified for 7 d at 4 °C and in the absence of light. Plants were grown in growth chambers set at long-day conditions (16 h light/8 h dark) under LED lights (intensity of 70 µmol m^{-2} s^{-1} and available spectra varying from 380 nm to 780 nm), a temperature of 22 °C, and ambient humidity. All lines were grown on soil (VPL-D-Arabidopsis 49144, Lensi Substrates, the Netherlands) except for the experiment in which flowering time was investigated. In this case, plants were grown on rockwool plugs in a separate growth chamber set at long-day conditions under LED lights, a temperature of 20 °C, and ambient humidity, and plants were fertilized bi-weekly with a 1 g l^{-1} Hyponex NPK 6.5-6-19 fertilizer (Hyponex, Japan).

Vector construction and transformation

The Golden Gate Molecular Cloning (MoClo) toolkit (Weber *et al.*, 2011) was utilized to assemble CRISPR/Cas9 constructs with the Golden Gate cloning strategy. Primers used for the design and sequencing of the CRISPR/Cas9 constructs are listed in Supplementary Table S1. Single guide RNAs (sgRNAs) targeting the *FT*, the *TFL1*, or the *bZIP67* gene were designed with the help of the CRISPR-P 2.0 tool (Liu *et al.*, 2017). The design parameters included the SpCas9 NGG PAM sequence, the U6 snoRNA promoter, a guide length of 20 bp, and the Arabidopsis target genome. Additionally, CRISPOR (Concordet and Haeussler, 2018) was used as a secondary reference to identify sgRNAs with high specificity scores, high predicted efficiency, and low off-target scores. Guides with high on-target efficiency and low off-target scores were carefully selected as the best candidates. Four sgRNAs were used to target *FT*, *TFL1*, or *bZIP67* exonic regions. The Arabidopsis U626 constitutive promoter was used to drive each guide. The resulting CRISPR/Cas9 constructs contained the four *pU626:sgRNAs* along with the *pOLE1:OLE1-RFP* (FAST-Red) plant selection marker and *pRPS5A:AtCas9* (Supplementary Table S2).

The MoClo toolset was also employed to assemble transcriptional (*pFT:GUS:tFT* and *pTFL1:GUS:tTFL1*) and translational (*pFT:FT-GFP:tFT* and *pTFL1:TFL1-GFP:tTFL1*) reporter lines. When needed, internal Golden Gate restriction sites were removed. Primers used for amplification, plasmid construction, and sequencing can be found in Supplementary Table S3.

For the *FT* transcriptional and translational reporter lines, the promoter and terminator regions of *FT* (–7267 to –1 and +2180 to +3676, respectively; initial nucleotide of the translational start as +1) were successfully amplified from L*er* genomic DNA. These products were inserted into pGEM®-T Easy Vectors (Promega) according to the manufacturer's instructions. Subsequently, those were introduced into the pL0 vectors pICH41295 and pICH41276, respectively. The *FT* full-length ORF was amplified, and its stop codon was removed. The *FT* gene without a stop codon was fused to the green fluorescent protein gene (*GFP*) via restriction–ligation into the pICH41308 pL0 vector. The *β-glucuronidase* (*GUS*) gene was also amplified and inserted into a pICH41308 pL0 vector. To construct the *pFT:FT-GFP:tFT* translational vector, the three distinct pL0 vectors were combined into the pL1-F2 vector. The final pL2 vector contained a kanamycin-resistant gene for *in planta* selection and the pL1-F2 *pFT:FT-GFP:tFT* (Supplementary Table S2). To construct the *pFT:GUS:tFT* transcriptional line, pL0 vectors containing the promoter, the *GUS* gene, and the terminator region were combined into the pL1-F2 vector. The final binary pL2 vector contained a kanamycin-resistant gene for *in planta* selection and the pL1-F2 *pFT:GUS:tFT* (Supplementary Table S2).

For the *TFL1* transcriptional and translational reporter lines, the promoter and terminator regions of *TFL1* (–2160 to –1 and +1037 to +5667, respectively; initial nucleotide of the translational start as +1) were successfully amplified from L*er* genomic DNA. These products were inserted into pGEM®-T Easy Vectors (Promega) according to the manufacturer's instructions. Subsequently, those were introduced into the pL0 vectors pICH41295 and pICH41276, respectively. The *TFL1* full-length ORF was amplified, and its stop codon was removed. The *TFL1* gene without a stop codon was fused to *GFP* via restriction–ligation into the pICH41308 pL0 vector. To construct the *pTFL1:TFL1-GFP:tTFL1* translational vector, the three distinct pL0 vectors were combined into the pL1-F2 vector. The final pL2 vector contained a kanamycin-resistant gene for *in planta* selection and the pL1-F2 *pTFL1:TFL1-GFP:tTFL1* (Supplementary Table S2). To construct the *pTFL1:GUS:tTFL1* transcriptional line, pL0 vectors containing the promoter region, the *GUS* gene, and the terminator region were combined into the pL1-F2 vector. The final binary pL2 vector contained a kanamycin-resistant gene for *in planta* selection and the pL1-F2 *pTFL1:GUS:tTFL1* (Supplementary Table S2).

Bacterial and plant transformation and selection

The *Escherichia coli* strain DH5α was used for the cloning of all constructs. In each cloning step, the presence of the correct plasmids was verified via restriction digestion and Sanger sequencing by the Macrogen Sequencing Service (Macrogen, Amsterdam, the Netherlands). All generated constructs were transformed into *A. tumefaciens* C58C1. Arabidopsis L*er* plants were floral dipped with C58C1 containing the appropriate plasmid. Transgenic T_0 seeds bearing the CRISPR/Cas9 constructs were selected using the FAST-Red selection marker. Red fluorescent protein (RFP) fluorescence was detected with the Leica MZ16F fluorescence microscope and a DSR filter (510–560 nm). CRISPR/Cas9 transgenic plants were screened for the presence of *FT*, *TFL1*, or *bZIP67* mutations. Young leaves were sampled and directly used for targeted amplification of genomic DNA via the Phire Plant Direct PCR Kit (Thermo Fisher Scientific). Amplified regions were sequenced by the Macrogen Sequencing Service (Macrogen, Amsterdam, the Netherlands). Sequencing data were analyzed using SnapGene (Dotmatics) and ICE synthego (Conant *et al.*, 2022) software. Three homozygous independent mutant plants lacking the T-DNA insertion were selected and used for further study. Primers used for generating the mutant lines can be found in Supplementary Table S4. Transgenic seeds containing the transcriptional and translational reporter constructs

were selected by selective germination and segregation analysis on medium with kanamycin (25 μg l^{-1}).

Flowering time analyses

Wild-type L*er* and single *ft* and *tfl1* mutant S_3 plants were phenotyped for flowering time. Flowering time was scored by counting the number of rosette leaves at the moment of visual bolting. Approximately 20 plants per genotype were scored.

Seed germination assays

Germination of wild-type L*er*, single and double *ft tfl1* mutant, and *bzip67* mutant S_4 (fourth generation by self-fertilization) seeds was assessed. The seeds were harvested from individual siliques on the primary inflorescence immediately upon dehiscence. Subsequently, these seeds were used for the germination assays. For each genotype, four biological replicates were sown once per week over 3–4 consecutive weeks. Each biological replicate consisted of seeds obtained from five distinct plants. During the period of dry storage, mature dry S_4 seeds were kept under semi-controlled conditions with a temperature range of 20–21 °C and ambient humidity.

Germination assays were performed using the Germinator package (Joosen *et al.*, 2010). Approximately 100 seeds per replicate were sown on two layers of blue germination paper. Germination papers were placed in plastic trays containing 42 ml of demineralized water. Multiple trays were stacked and placed inside transparent plastic bags. Plastic bags containing the trays were incubated at a constant temperature of 22 °C under continuous light (Incubator Snijders EB2-N with white LED lights 4000K). Each germination experiment was monitored for 7 d by taking pictures. Germination was scored as radicle emergence.

Seed quality traits t_{50} (time to 50% germination) and uniformity (measured using the U_{8416} parameter, defined as the time interval between 16% and 84% germination) were assessed based on the germination data of fully matured S_4 seeds. These measurements were calculated using the curve-fitter module of the Germinator package (Joosen *et al.*, 2010). Each genotype contained at least three biological replicates, each consisting of seeds from five different plants.

Seed size determination

Mature dry S_4 seeds of wild-type L*er* and single and double *ft tfl1* mutants were used for seed size determination. Plants were photographed, and seed area (mm^2) was calculated by using the ImageJ1.40 software. The weight of the dry seeds (mg) was also measured. Per genotype, 3–4 biological replicates were used. Each replicate contained at least 80 seeds from five different plants.

Microscopy and imaging

For *pFT:GUS:tFT* and *pTFL1:GUS:tTFL1*, GUS activity was determined as previously reported (Song *et al.*, 2019). Whole rosette, whole inflorescence, siliques, or dissected seeds at different developmental stages were incubated in the staining solution at 37 °C for 1 h, 2 h, or overnight. After incubation, the stained tissues were placed in clearing solution (chloral hydate:water:glycerol 8:3:1) prior to analysis with differential interference contrast (DIC) imaging via a Nikon Optiphot microscope. Images were taken with a Zeiss Axiocam 105 camera (Willemsen *et al.*, 1998).

For *pFT:FT-GFP:tFT* and *pTFL1:TFL1-GFP:tTFL1*, tissue fixation was carried out as previously described (Attuluri *et al.*, 2022). In brief, the fixation of the material was performed using a solution consisting of 4% paraformaldehyde in 1× phosphate-buffered saline (PBS) with 0.05% Triton X-100 (PBS-T). Siliques at specific embryonic developmental stages were opened and placed in a 12-well plate containing the fixative solution. Throughout the procedure, the plate was covered with aluminum foil to ensure the tissues were shielded from light. To eliminate air bubbles, the samples were vacuum infiltrated for ~30 min on ice. Subsequently, these were incubated overnight at 4 °C with gentle rotation. On the following day, the samples were washed three times with 1× PBS-T at room temperature, with each wash lasting 1 h. Following fixation, the samples were cleared by shaking in the presence of ClearSee alpha solution. This solution was prepared as described by Kurihara *et al.* (2021) and supplemented with 50 mM sodium sulfite as an antioxidant agent. The clearing process was extended for a minimum of 2 months. After this period, a Leica SPE DM5500 confocal microscope was used to visualize GFP in the fixated and cleared material. GFP was excited at 488 nm and detected at 470–550 nm.

Yeast two-hybrid assay

The bait vectors BD-FT and BD-TFL1 were transformed into the yeast strain PJ69-4α using the small-scale yeast transformation method (de Folter and Immink, 2011). Subsequently, individual colonies from both the BD-FT and BD-TFL1 transformations were suspended in 50 μl of sterile Milli-Q water and tested for autoactivation by spotting onto plates of synthetic dropout medium (SD) lacking leucine (L) and histidine (H) and supplemented with 1, 5, or 10 mM 3-amino-1,2,4-triazole (3-AT). Following a 5 d incubation at 20 °C, yeast growth and hence autoactivation were assessed, revealing the absence of autoactivation capacity of FT and TFL1. Subsequently, a matrix-based protein–protein interaction assay was performed, in which FT and TFL1 were screened against 64 members of the Arabidopsis bZIP transcription factor family as previously described (de Folter and Immink, 2011; Pruneda-Paz *et al.*, 2014). After mating, the diploid yeast was spotted onto selective medium lacking L, tryptophan (W), and H and supplemented with 1 mM or 5 mM 3-AT. The interaction plates were incubated for 5 d at 20 °C. Two technical replicates using two different handpicked colonies from the BD-FT and BD-TFL1 transformations were performed.

RNA extraction

Plant material was sampled between 2 h and 4 h before dusk. For the gene expression analysis, RNA was isolated from *ft-cr3*, *tfl1-cr2*, and wild-type L*er* dissected siliques (without seeds) and seeds at the torpedo stage of embryo development. For the RNA-seq study, RNA was isolated from wild-type L*er* seeds at the torpedo stage of embryo development. Per genotype, we sampled three biological replicates each consisting of 6–7 dissected siliques or seeds from 6–7 individual plants.

For dissected siliques, total RNA was extracted using the InviTrap® Spin Plant RNA Mini kit (Invitek diagnostics). For seeds, total RNA was extracted using the hot borate protocol described by Maia *et al.* (2011). In summary, seeds were combined with 800 μl of extraction buffer containing DTT and polyvinylpyrrolidone 40 (PVP40), which had been heated to 80 °C. Proteinase K was added and the mixture was incubated for 15 min at 42 °C. After the addition of 2 M KCl, the samples were incubated on ice for 30 min and then centrifuged. Ice-cold 8 M LiCl was added to the supernatant, and the tubes were incubated overnight on ice. Following centrifugation, the resulting pellets were washed with ice-cold 2 M LiCl and centrifuged for 10 min. The pellets were resuspended in 80 μl of diethylpyrocarbonate (DEPC)-treated water. Subsequently, the samples were subjected to phenol–chloroform extraction, DNase treatment using RQ1 DNase (Promega), and purification.

Gene expression analyses

cDNA synthesis was conducted using the iScript cDNA synthesis kit (BioRad). For quantitative real-time PCR (qRT-PCR) analysis, a 10 μl

reaction volume was prepared, consisting of 5 µl of iQ™ SYBR® Green Supermix (Bio-Rad), 2.5 µl of template cDNA, 0.12 µl of each primer (10 µM), and 2.25 µl of Milli-Q water. The amplification was assayed on the Bio-Rad CFX96. Relative gene expression was calculated according to the $2^{-\Delta\Delta CT}$ method (Livak and Schmittgen, 2001) using wild-type samples as the calibrator and the *TIP41* family gene (*AT4G34270*) as the reference. On the basis of its ubiquitous expression, *TIP41* has been widely used as the reference in gene expression studies (Czechowski *et al.*, 2005). Primers used are shown in Supplementary Table S5.

Library preparation and RNA-seq analysis

Library preparation and RNA sequencing (non-stranded, paired-end 150, Illumina NovaSeq 6000) were outsourced to Novogene. The raw sequencing data are available from NCBI's Sequence Read Archive (BioProject PRJNA1054800).

Following high-throughput sequencing, paired-end reads were trimmed using Trimmomatic version 0.39 (Bolger *et al.*, 2014) with settings: 'ILLUMINACLIP:TruSeq3- PE.fa:2:30:10:2:True LEADING:3 TRAILING:3 MINLEN:36'. The resulting trimmed reads were aligned to the TAIR10 Arabidopsis genome, using HISAT version 2.2.1 (Kim *et al.*, 2019). Assembly and quantification of the transcripts was done using StringTie version 2.2.1 (Pertea *et al.*, 2015) with the Araport11 genome annotation (version February 2022) and the -e, -B, and -G options, followed by aggregation to gene-level counts with StringTie's prepDE script. Genes with a maximum read count per sample <10 were removed. Differentially expressed genes (DEGs) were identified with the Differential Expression for Sequence Count Data 2 (DESeq2) R package from Bioconductor using the nbinomWaldTest function with default parameters (Love *et al.*, 2014).

Quantification and statistical analyses

Statistical significance was determined using the RStudio software. The number of samples analyzed is specified in the method details. The figure legends describe the relevant statistical test employed. Data are presented as means ±SD, except for the expression analysis, where the data are represented as means ±SE.

Results

Arabidopsis L*er FT* and *TFL1* knockout lines show a flowering time and inflorescence phenotype

In the Arabidopsis L*er* background, *ft* and *tfl1* mutants are known that harbor mutations introducing premature stop codons later in the coding sequence (Alvarez *et al.*, 1992; Kardailsky *et al.*, 1999). For instance, the *ft-2* mutant, generated by ethyl methanesulfonate (EMS) mutagenesis, contains a single nucleotide substitution, which introduces a stop codon at amino acid 138 while preserving the integrity of the first three exons (Kardailsky *et al.*, 1999). To investigate the potential involvement of *FT* and *TFL1* in seed quality, we generated *de novo* Arabidopsis L*er FT* and *TFL1* mutants by targeted mutagenesis using CRISPR/Cas9 technology. These new mutants were specifically engineered to introduce early stop codons and produce full knockout alleles, thereby facilitating a more comprehensive analysis of their functional contributions. For *FT*, four guide sequences (sgRNA1–sgRNA4) were designed to target the first, second, and third exons (Supplementary Fig. S1A). For *TFL1*, the four guide sequences were distributed between the first and the second exons (Supplementary Fig. S1B). Three independent homozygous mutations at the *AtFT* and *AtTFL1* loci were selected. *ft* lines #1 and #3 (hereafter *ft-cr1* and *ft-cr3*) exhibit a single nucleotide insertion and a single nucleotide deletion, that resulted from successful cleavage at the sgRNA2 and sgRNA1 sites, respectively. *ft* line #2 (hereafter *ft-cr2*) shows a 159 bp deletion, which resulted from successful cleavage between the sgRNA1 and sgRNA2 sites, and a 1 bp deletion, which resulted from successful cleavage at the sgRNA4 target site. *tfl1* lines #1, #2, and #3 (hereafter *tfl1-cr1*, *tfl1-cr2*, and *tfl1-cr3*) exhibit deletions of different lengths. *tfl1-cr1* presents a 1 bp deletion at the sgRNA2 and sgRNA3 sites. *tfl1-cr2* and *tfl1-cr3* show a 13 bp and 4 bp deletion, respectively, which resulted from successful cleavage at the sgRNA2 site. In nearly all cases, the polymorphisms lead to frameshift mutations in the *FT* or *TFL1* locus, which ultimately will result in truncated proteins when the modified RNAs are translated (Supplementary Fig. S2).

The *PEBP* genes *FT* and *TFL1* have well-established roles in the regulation of flowering time and meristem development (Moraes *et al.*, 2019). To validate the CRISPR-generated null lines, we assessed their flowering time and examined the architecture of their inflorescences (Supplementary Fig. S1C, D). As expected, the loss of function of *FT* resulted in a late-flowering phenotype with plants containing >20 rosette leaves at the moment of bolting. Conversely, loss of function of *TFL1* resulted in an early-flowering phenotype, with plants having <10 rosette leaves (Supplementary Fig. S1C). Inflorescence development effects were also observed in all mutant lines. While *ft-cr* mutants increased their vegetative growth and axillary meristems gave rise to lateral shoots, *tfl1-cr* mutants contained relatively short primary and secondary inflorescences that ended in a terminal floral structure (Supplementary Fig. S1D). Taken together, these observations reveal the anticipated phenotypic alterations in flowering time and inflorescence architecture, and thereby confirm the validity of the generated *FT* and *TFL1* knockout lines for further functional characterization.

FT and *TFL1* loss-of-function mutants exhibit altered seed dormancy

Seed vigor is a multifaceted trait that encompasses various attributes crucial for successful seed performance (Reed *et al.*, 2022). Among these key attributes are seed dormancy, viability, rapid germination, and seedling establishment, particularly in suboptimal conditions. To examine the potential involvement of *FT* and *TFL1* genes in these essential characteristics, we subjected the generated *ft-cr* and *tfl1-cr* lines to different tests. Firstly, these mutants were investigated for their dormancy phenotypes. In a study conducted by Chen *et al.* (2014), the dormancy phenotype of three *ft* mutants (*ft-1*, *ft-2*, and *ft-3*) generated through EMS mutagenesis was

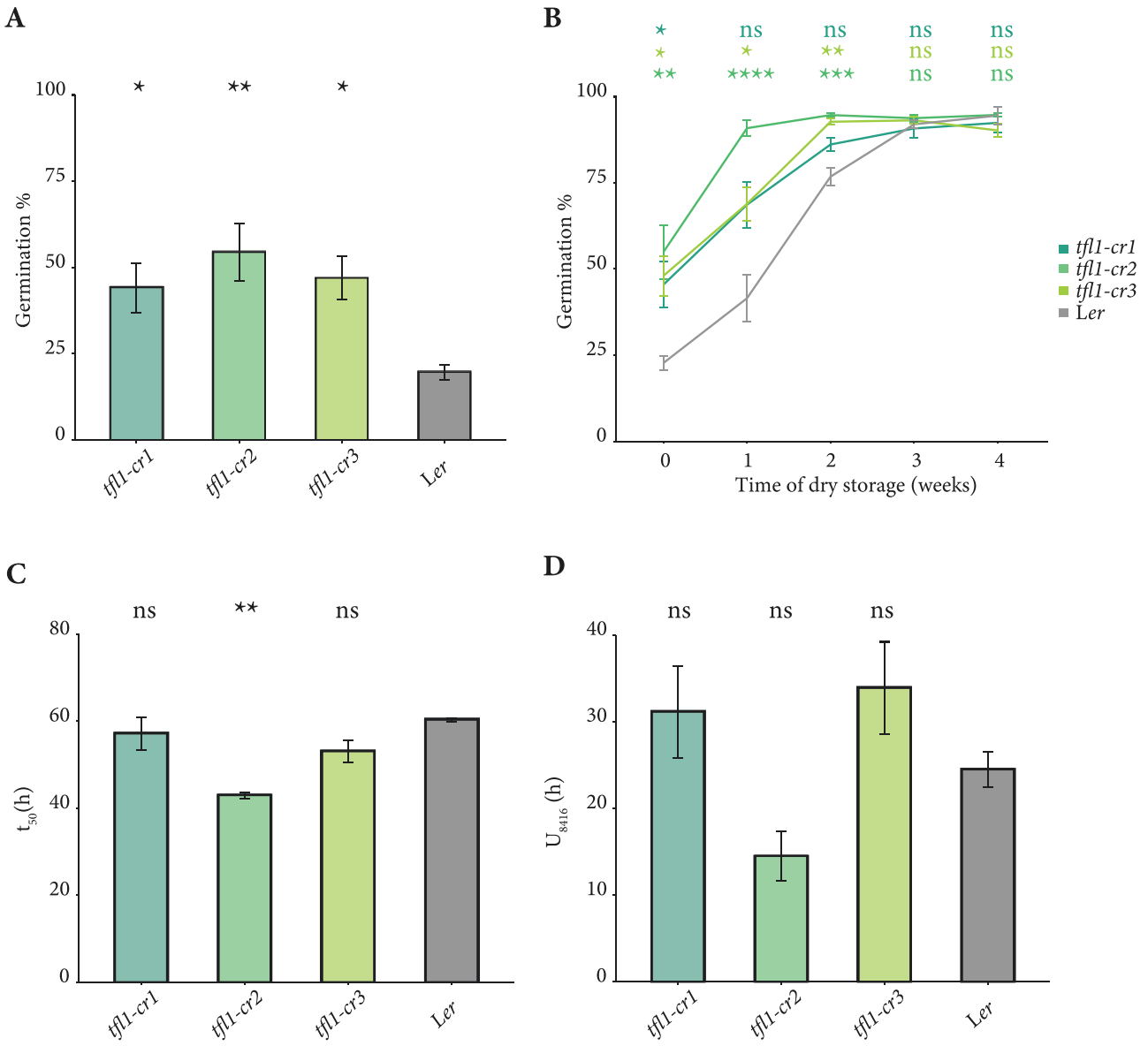

Fig. 1. Germination analysis of *tfl1* CRISPR/Cas9 mutants. (A) Germination of freshly harvested seeds from plants grown at continuous 22 °C scored 7 d after sowing. Dormancy is assessed by evaluating the germination percentage 7 d after sowing freshly harvested seeds. The lower the germination percentage, the higher the dormancy level. (B) Summary of germination results scored after several weeks of dry storage of seeds from plants grown at continuous 22 °C. (C) Time to reach 50% germination (t_{50}) or germination speed of fully matured seeds from plants grown at continuous 22 °C. (D) Uniformity or time interval between 16% and 84% germination (U_{8416}) of fully matured seeds from plants grown at continuous 22 °C. (A–D) Per genotype, 3–4 biological replicates that include seeds from five different plants were tested. Asterisks indicate statistically significant differences compared with the wild-type L*er* using a Dunn test (A, B, D) and a TukeyHSD test (C). ns (not significant); $P>0.05$; *$P<0.05$; **$P<0.01$; ***$P<0.001$, ****$P<0.0001$.

already analyzed. However, these mutants only exhibited alterations in the last exon of the *FT* gene. Yet, *FT* was identified as a positive regulator of seed germination. For comparative purposes, we used the *ft-1* line as a control in our study. Following the previously published data, freshly harvested *ft* mutant seeds showed a deeper primary dormancy level than wild-type L*er* (Supplementary Fig. S3A). This initial dormancy depth was subsequently lost after 4 weeks of dry seed storage (Supplementary Fig. S3B). These results provide further evidence supporting the role of *FT* in controlling seed dormancy. Interestingly, and in contrast to the *ft* mutant lines, freshly harvested seeds for all three *tfl1-cr* mutants exhibited a notable reduction in seed dormancy when compared with wild-type L*er* (Fig. 1A, B). In these lines, the initial depth of dormancy diminished progressively over time, and total germination was achieved 3 weeks after storage. Collectively, these findings reveal a previously unknown role for *TFL1* in the induction and maintenance of seed dormancy.

To gain further insights into how *ft* and *tfl1* mutants influence the overall germination process, we examined various parameters associated with rapid and synchronized germination in fully after-ripened seeds. The speed of germination or germination rate was quantified via the t_{50} metric, which indicates the time required to reach 50% germination. In general, alterations in the *FT* gene exhibited a substantial impact on the t_{50}. All *ft* mutant seeds, except for *ft-cr2*, displayed a decrease in germination speed when compared with the wild type (Supplementary Fig. S3C). In contrast, mutations in the *TFL1* gene did not have any impact on this parameter, except for the *tfl1-cr2* line. This particular mutant reached 50% germination ~20 h earlier than the wild-type L*er* (Fig. 1C; Supplementary Fig. S3C). Lastly, uniformity, or U_{8416}, defined as the time interval between 16% and 84% germination, was tested. Overall, we did not observe significant differences in the uniformity of germination of *ft* and *tfl1-cr* mutant seeds (Fig. 1D' Supplementary Fig. S3D). This indicates that the germination process was relatively consistent across all tested samples.

Collectively, these findings highlight the role of both *FT* and *TFL1* genes in controlling a range of characteristics linked to optimal seed performance. Mutations in *FT* increase dormancy and decrease germination speed, while mutations in *TFL1* reduce dormancy.

TFL1 loss-of-function mutants display a significant increase in seed size, an *FT* loss-of-function mutants show minor effects

Seed development plays a crucial role in shaping the evolutionary fitness and crop yield of flowering plants. Numerous growth parameters contribute to the overall process of seed development. Among these parameters, seed size stands out as a significant factor closely linked to nutrient levels necessary for germination, and the seed's ability to withstand abiotic stress during the establishment of seedlings (Moles *et al.*, 2005). Based on a recent study that reported *TFL1* as an essential player in the determination of Arabidopsis seed size (Zhang *et al.*, 2020), we decided to quantify seed size in our set of mutants. In line with those observations, both seed mass and area were remarkably increased in our *TFL1* loss-of-function mutants, *tfl1-cr1*, *tfl1-cr2*, and *tfl1-cr3* (Fig. 2A, B). In contrast to *TFL1*, the *FT* loss-of-function mutants exhibited only minor effects on seed size. Although the mean weight of 100 seeds did not show significant differences compared with the L*er* wild type, *ft-cr* mutants did display a significantly larger surface area (Fig. 2C, D).

FT and *TFL1* expression patterns in Arabidopsis reproductive tissue

Thus far, we have observed that both *FT* and *TFL1* play a role in regulating various seed quality characteristics including dormancy, germination speed, and size. To understand whether these genes exhibit a comparable spatial distribution in the reproductive tissue of Arabidopsis—namely inflorescence, silique, funiculus, and seed—we generated *pFT:GUS* and *pTFL1:GUS* reporter lines. For this purpose, the *GUS* gene was encased between a 7.2 kb or 2.2 kb endogenous *FT* or *TFL1* promoter fragment, respectively, and a 1.5 kb or 4.6 kb endogenous *FT* or *TFL1* terminator fragment, respectively (Supplementary Fig. S4A). In total, we obtained 19 independent *pFT:GUS* and 22 independent *pTFL1:GUS* lines. These lines were validated by confirming the presence of specific GUS staining in the SAM of *pTFL1:GUS*, and in the leaf vasculature of *pFT:GUS* (Supplementary Fig. S4B, C) (Simon *et al.*, 1996; Bradley *et al.*, 1997; Ratcliffe *et al.*, 1999; Takada and Goto, 2003). Subsequently, a representative line per construct was selected to monitor the detailed localization of both *FT* and *TFL1* in reproductive tissues. Analyses of these reporter lines revealed both *pFT* and *pTFL1* activity in Arabidopsis inflorescences (Fig. 3A, C). In both cases, GUS was also detected in the funiculus (Fig. 3B, D). Next, we examined *FT* and *TFL1* spatial patterns in seeds and connecting tissues at distinct stages of development. *pFT:GUS* and *pTFL1:GUS* activities were consistently localized at the vascular bundle, phloem unloading region, and chalazal seed coat in all the stages analyzed (Fig. 3F, G, I). Additionally, seeds bearing *pTFL1:GUS* showed specific expression inside the seed at the chalazal endosperm, located above the maternal barrier, at a short developmental time span (Fig. 3F, H), as had previously been reported (Zhang *et al.*, 2020). Remarkably, no GUS signal was detected in this particular area in plants harboring *pFT:GUS* (Fig. 3F, J). Taken together, these findings indicate that before flowering *FT* and *TFL1* are situated in the leaf and SAM, respectively. However, after flowering, they are not only expressed in different locations within the maternal–filial boundaries, but they also co-localize in some of these reproductive maternal tissues. Precisely during the reproductive stages, *FT* is exclusively present in maternal tissues both before and after fertilization, while *TFL1* is found both in maternal tissues before and after fertilization, as well as in endosperm tissue at early stages of seed development.

FT protein is localized within the phloem unloading zone

Both FT and TFL1 proteins are well-established mobile elements involved in the control of flowering time. In the vegetative stage of development, FT is produced in the leaf companion cells and travels long distances through the sieve elements to eventually reach the shoot apex (Wigge, 2011). In contrast, TFL1 exhibits shorter range movement by traveling from the center of the SAM to the outer L1 meristem layer (Conti and Bradley, 2007). Recent research by Zhang *et al.* (2020) has provided novel insights into the spatial distribution of TFL1 in seeds. Intriguingly, the movement of this protein goes beyond the confines of the apical meristem by

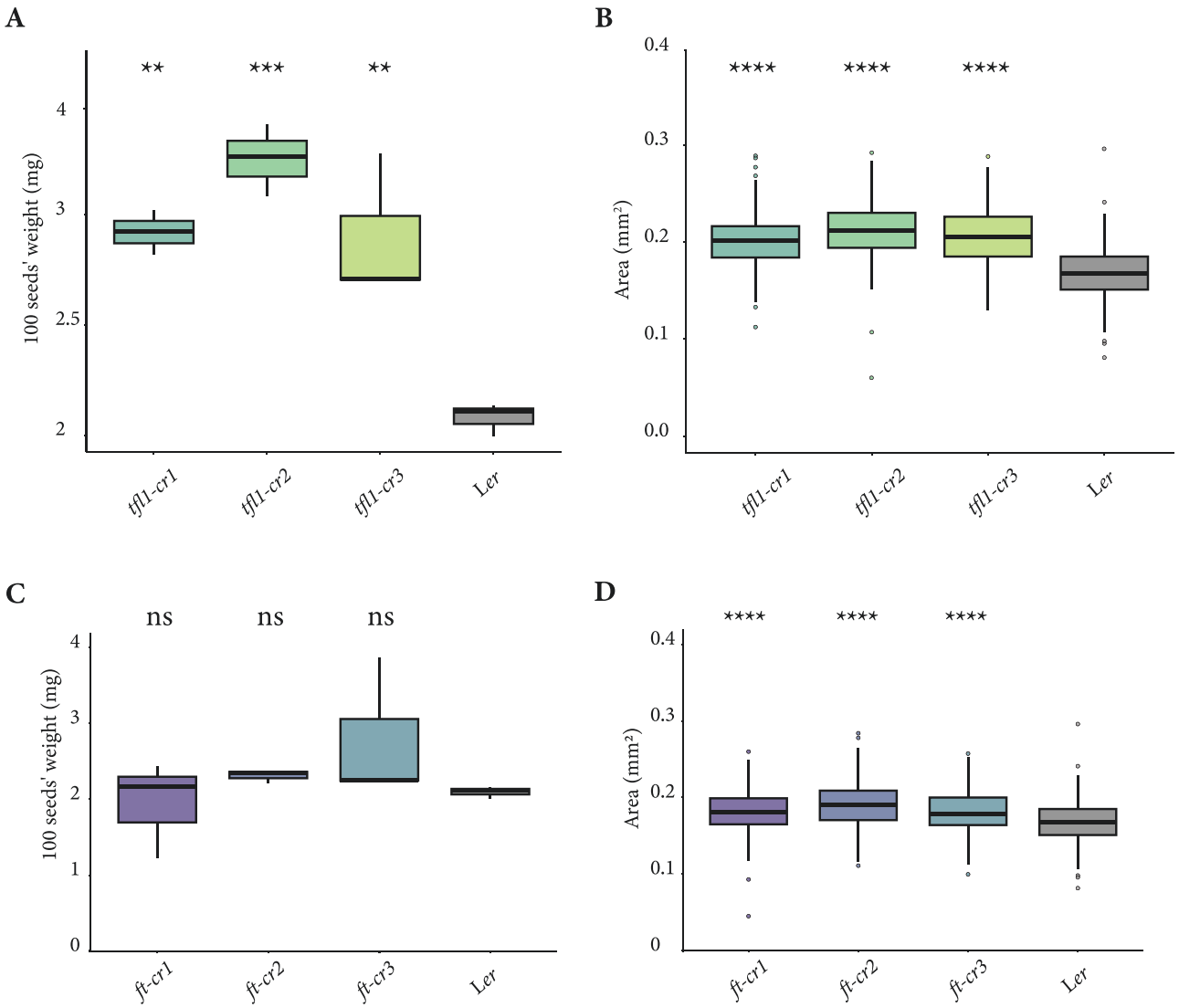

Fig. 2. Seed size determination of *tfl1* and *ft* CRISPR/Cas9 mutants. Quantitative analysis of seed mass measured as 100-seed weight in *tfl1-cr* (A) and *ft-cr* (C) mutants. Quantitative analysis of seed size measured as area in *tfl1-cr* (B) and *ft-cr* (D) mutants. (A–D) Per genotype, three biological replicates each including at least 80 seeds from five different plants were tested. Asterisks indicate statistically significant differences compared with the wild-type L*er* using a TukeyHSD test (A, C) and a Dunn test (B, D). ns (not significant) $P>0.05$; *$P<0.05$; **$P<0.01$; ***$P<0.001$, ****$P<0.0001$.

serving as a mobile regulator to facilitate the proper development of the seed. Within this tissue, *TFL1* originates in the chalazal endosperm of torpedo-stage embryos and its protein is found in the peripheral endosperm where it mediates the timing of endosperm cellularization and, as such, final seed size. Given the mobile nature of these proteins at various stages of the plant's life cycle, we examined whether FT could also travel within or between maternal and filial seed regions. For that, we generated three independent *pFT:FT-GFP:tFT* lines where the *FT* ORF was fused to GFP and was expressed under the endogenous *FT* promoter and terminator (Supplementary Fig. S5A). In general, the localization of the FT–GFP signal was consistent with the histochemical GUS studies representing promoter activity (Fig. 3I, J). FT–GFP could be detected at the septum (Fig. 4A). The FT–GFP protein was also abundantly detectable in the vascular tissue of the funiculus and at the phloem unloading area (Fig. 4A, B). Furthermore, at least three independent *pTFL1:TFL1-GFP:tTFL1* lines showed the presence of TFL1–GFP signal within the vascular bundles of the funiculus and phloem unloading area (Supplementary Fig. S5B).

Next, FT localization was examined in seeds at different developmental stages. Consistently, the FT–GFP signal was detected at the vascular and unloading area at all stages analyzed (Fig. 4C, D).

Taken together, we could not detect any FT protein movement between maternal and filial seed tissues above the detection limit for GFP at the investigated developmental stages.

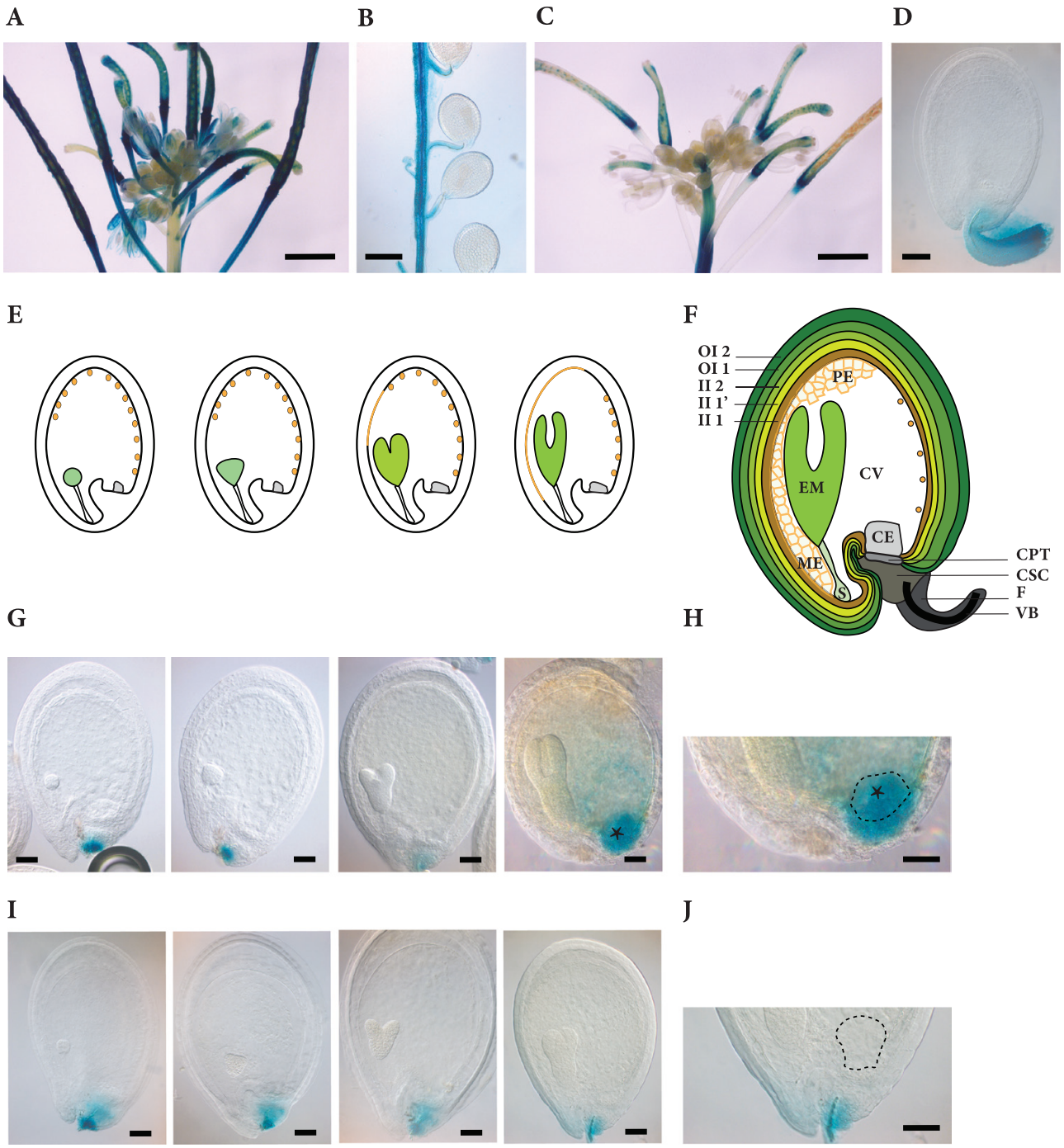

Fig. 3. Localization of *pFT:GUS* and *pTFL1:GUS* activity in reproductive tissue. (A) GUS staining of a *pFT:GUS* inflorescence. Scale bar, 1 mm. (B) GUS staining of a *pFT:GUS* seed attached to the septum via the funiculus. Scale bar, 30 µm. (C) GUS staining of a *pTFL1:GUS* inflorescence. Scale bar, 1 mm. (D) GUS staining of a *pTFL1:GUS* seed with funiculus. Scale bar, 100 µm. (E) Schematic representation of developing seeds. From left to right: globular, triangular, heart, and torpedo stages. (F) Schematic representation of a seed at the torpedo stage of embryo development. Arabidopsis seed anatomy after Debeaujon *et al*. (2003): OI 2, outer layer of the outer integument; OI 1, inner layer of the outer integument; II 2, outermost layer of the inner integument; II 1', middle layer of the inner integument; II 1, innermost layer of the inner integument (endothelium); CV, central vacuole; EM, embryo; S, suspensor; ME, micropylar endosperm; PE, peripheral endosperm; CE; chalazal endosperm; CPT, chalazal proliferating tissue; CSC, chalazal seed coat; F, funiculus; VB, vascular bundle. (G) GUS staining of *pTFL1:GUS* developing seeds. The black asterisk indicates *pTFL1:GUS* signal in chalazal endosperm. From left to right, early globular embryo to torpedo embryo stage. Scale bar, 100 µm. (H) Zoom in of the basal part of a *pTFL1:GUS* seed at the torpedo stage of embryo development. The dashed line encloses the chalazal endosperm. The black asterisk indicates *pTFL1:GUS* signal in chalazal endosperm. Scale bar, 100 µm. (I) GUS staining of *pFT:GUS* developing seeds. From left to right, early globular embryo to torpedo embryo stage. Scale bar, 100 µm. (J) Zoom in of the basal part of a *pFT:GUS* seed at the torpedo stage of embryo development. The dashed line encloses the chalazal endosperm. Scale bar, 100 µm.

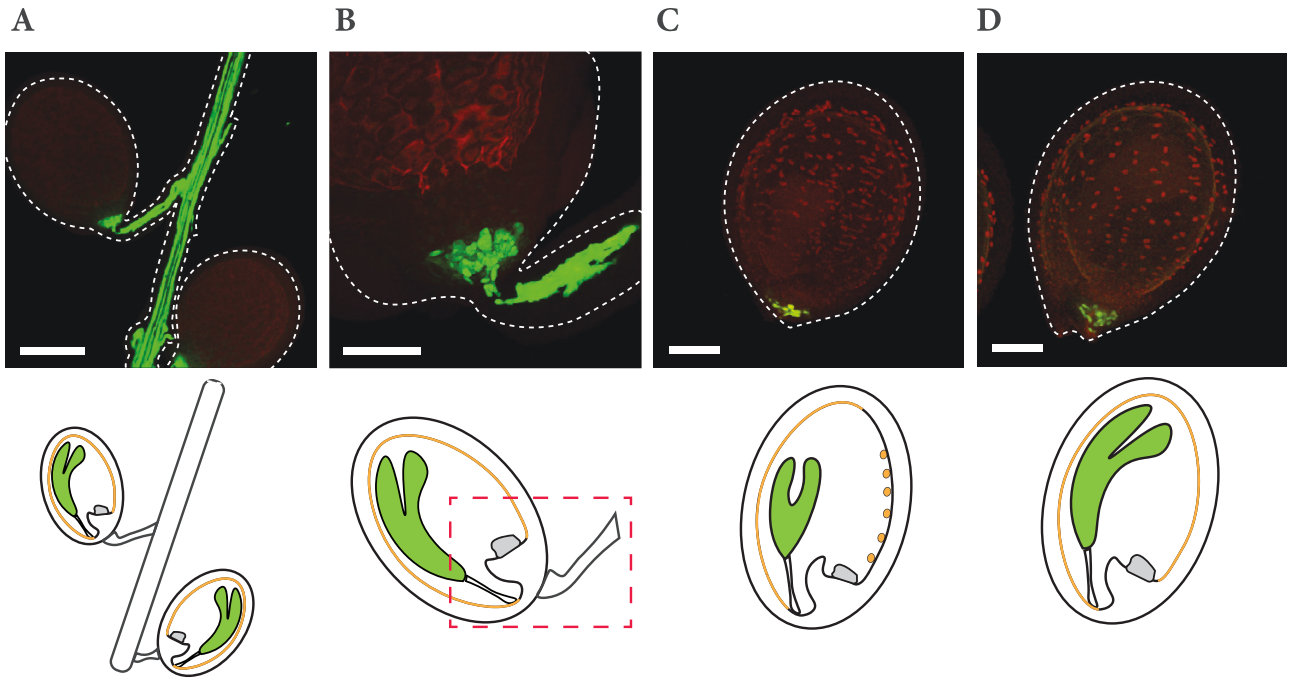

Fig. 4. Localization of *pFT:FT-GFP* signal in reproductive tissues. (A) Confocal images of *pFT:FT-GFP* in developing seeds still attached to the mother plant (septum) via the funiculus. Scale bar, 0.25 mm. (B) Zoom in on the funiculus and basal part of *pFT:FT-GFP* developing seeds. Scale bar, 75 µm. (C and D) Confocal images of *pFT:FT-GFP* in developing seeds with embryos at the torpedo (C) and bent (D) stages of development. Scale bar, 100 µm. (A–D) Top: merged GFP (green) and autofluorescence (red), where the dashed lines indicate the seed shape. Bottom: schematic representation of presented tissues and seed developmental stages.

Instead, FT–GFP remained confined at the maternal vasculature and the vasculature unloading area. So, in contrast to what was observed for TFL1–GFP by Zhang *et al.* (2020), we could not detect FT–GFP in fertilization-derived seed tissues. Therefore, in seeds and connective tissues, FT and TFL1 proteins only partly co-localize in maternal regions and only TFL1 proteins seem to be present in offspring seed tissues and mobile within the endosperm tissue of the fertilized seeds.

Simultaneous loss of *FT* and *TFL1* shows a restoration of seed dormancy to wild-type levels and complex interactions in the determination of seed size and yield

So far, our observations have indicated that both *FT* and *TFL1* genes play a role in multiple aspects related to the overall seed quality (Figs 1, 2; Supplementary Fig. S3). Combined with their partial spatial overlap (Figs 3, 4), this suggests their interaction in certain aspects of seed development and maturation. Therefore, we next investigated the genetic relationship between *FT* and *TFL1* starting with their control of seed dormancy. To accomplish this, we generated the *ft tfl1* double mutant by crossing two of our single mutant lines. In accordance with our previous germination results, both single mutants showed opposite dormancy behavior (Fig. 5A). These dormancy phenotypes observed in *tfl1-cr2* and *ft-cr3* were lost after 1 or 4 weeks of dry storage, respectively (Fig. 5B). Remarkably, freshly harvested double *ft tfl1* mutant seeds restored the wild-type L*er* germination levels 7 d after sowing (Fig. 5A). The initial dormancy depth found both in the *ft tfl1* double mutant and in the wild type was lost at the same rate during dry seed storage. In fact, 3–4 weeks after harvest, both genotypes had completely lost all their dormancy and germinated close to 100% (Fig. 5B).

Subsequently, we investigated the genetic relationship between *FT* and *TFL1* in the control of seed size and seed yield. The seed area of the double *ft tfl1* mutant seeds exhibited an intermediate phenotype between *tfl1* and wild-type L*er*, whereas the 100-seed weight resembled the *tfl1* phenotype (Fig. 5C, D). This suggests that while mutations on the *FT* gene may not strongly impact seed size in the single mutant background, they exert a somewhat compensatory effect within the context of the *ft tfl1* double mutant background. Further examination of the single and double mutants revealed that *tfl1-cr2* seed number per silique was comparable with that of wild-type plants, as had been previously reported (Fig. 5E) (Zhang *et al.*, 2020). However, the total seed weight of seeds harvested from 10 plants (hereafter also total seed yield) was considerably decreased in this mutant (Fig. 5F). As for *ft-cr3*, seed number per silique was, on average, slightly lower than in the wild type. However, the total seed yield of 10 plants was significantly increased when compared with both *tfl1-cr2* and the wild type (Fig. 5E, F). Notably, the double *ft tfl1* mutant exhibited a significant reduction in the number of seeds per fruit, averaging ~10 seeds less than L*er* (Fig. 5E). Nevertheless, the total seed yield was more similar to that of the *ft-cr3* mutant

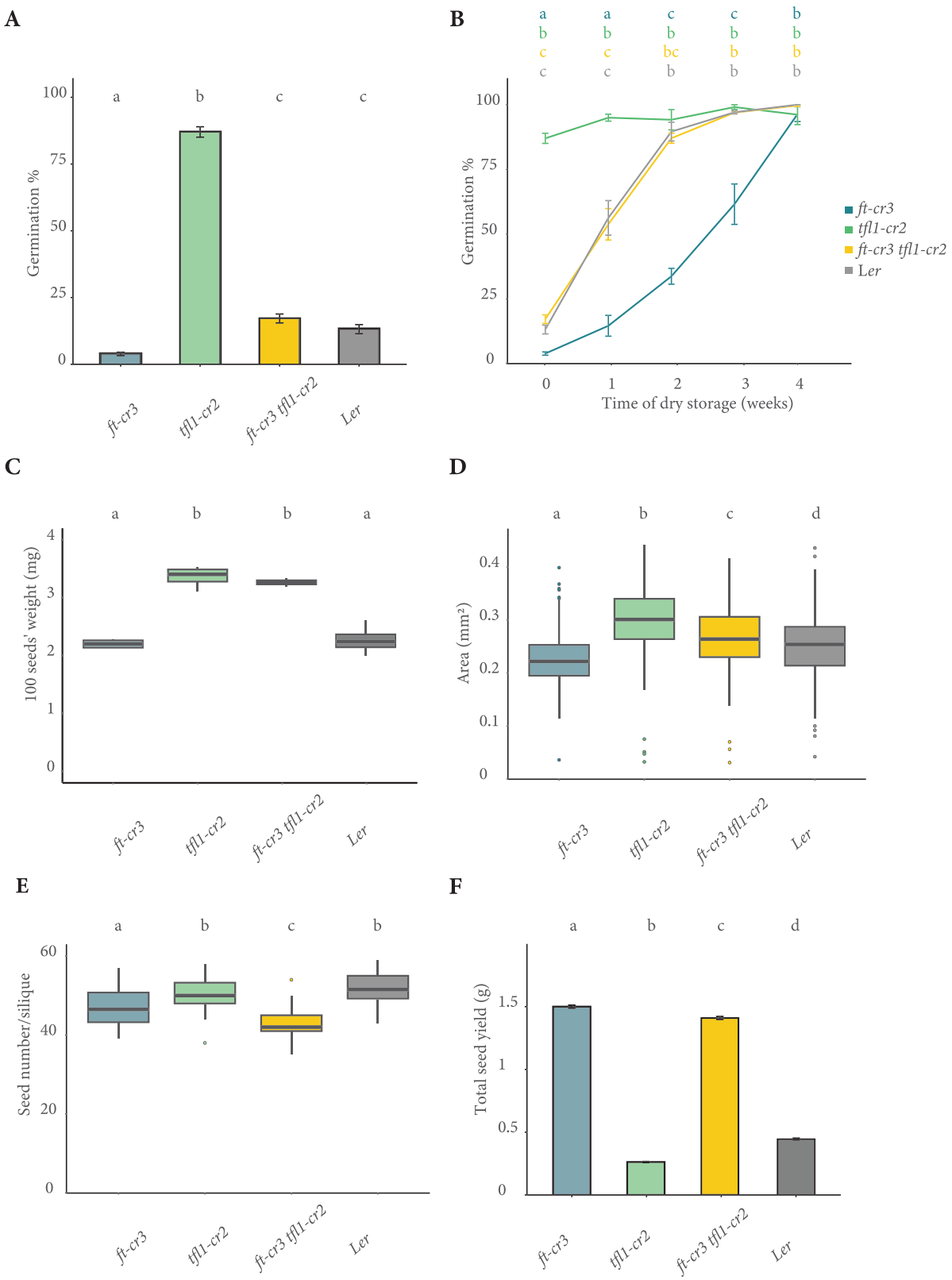

Fig. 5. Characterization of the seed dormancy, seed size, and seed yield traits in the *ft* and *tfl1* double mutants. (A) Germination of freshly harvested seeds from plants grown at continuous 22 °C scored 7 d after sowing. Dormancy is assessed by evaluating the germination percentage 7 d after sowing freshly harvested seeds. The lower the germination percentage, the higher the dormancy level. (B) Summary of germination results scored after several weeks of dry storage of seeds from plants grown at continuous 22 °C. (A and B) Per genotype, four biological replicates that include seeds from five different plants were

tested. (C) Quantitative analysis of seed mass measured as 100-seed weight of at least 80 wild-type L*er*, single, and double *ft tfl1* seeds. (D) Quantitative analysis of seed size measured as area of at least 80 wild-type L*er*, single, and double *ft tfl1* seeds. (C and D) Per genotype, four biological replicates that include seeds from five different plants were tested. (E) Comparison of seed number per silique. Per genotype, 30 siliques from six different plants were used. (F) Total seed weight per 10 plants or total seed yield. Per genotype, two biological replicates that include seeds from 10 different plants were quantified. (A–F) Lowercase letters indicate significant difference ($P<0.05$) using a TukeyHSD test (A, E, F) and a Kruskal–Wallis test adjusted with the Bonferroni correction (B, C, D). The same letters between groups indicate non-significant differences, and different letters between groups indicate significant differences.

(Fig. 5F). Summarizing, these observations reveal complex and dynamic interactions between *FT* and *TFL1* when it comes to seed dormancy, seed size, and total seed yield.

Molecular underpinnings of FT and TFL1 functions in seeds

Based on the results of Chen *et al.* (2014), it was suggested that the *ft-1* mutant exerts control over progeny dormancy by influencing proanthocyanidin (condensed tannins) synthesis in Arabidopsis fruits. In their study, an increase in the expression level of a selection of proanthocyanidin biosynthesis genes was observed in siliques of *ft* mutant plants. This observation prompted us to study the expression of *BANYULS* (*BAN*), *LEUCOANTHOCYANIDIN DIOXYGENASE* (*LDOX*), *DIHYDROKAEMPFEROL* (*DFR*), and *TRANSPARENT TESTA 10* (*TT10*) in *tfl1-cr2* dissected siliques and seeds. In line with the observed opposite effect of *FT* and *TFL1* on seed dormancy, we found down-regulation of the expression levels for most of these genes in siliques, but not significantly in seeds of *tfl1-cr2* plants (Fig. 6).

The expression analysis of the proanthocyanidin biosynthesis genes in siliques and the dormancy phenotyping both point towards an opposite functioning of *FT* and *TFL1* in the control of seed dormancy, as is seen in flowering time control and inflorescence architecture. For the latter two functions, this is thought to be accomplished by competition for interaction with the bZIP transcription factor FD (Zhu *et al.*, 2020). FD belongs to the A-subgroup of bZIP transcription factors. In Arabidopsis, the bZIP transcription factor family encompasses ~78 members, which are classified into 13 distinct groups. These transcription factors are involved in a wide range of functions, including developmental processes, abiotic responses, and stress signaling (reviewed in Dröge-Laser *et al.*, 2018; Guo *et al.*, 2024). These observations inspired us to investigate the breadth of interactions between the PEBP family members FT and TFL1, and members from the bZIP family of transcription factors. To do that, we made use of the GAL4 yeast two-hybrid (Y2H) assay. Neither FT nor TFL1 exhibited autoactivation when expressed from the GAL4-binding domain (BD). Therefore, combinations between FT or TFL1 proteins and bZIPs could be assessed for protein–protein interaction capacity. We tested a comprehensive set of 64 bZIP transcription factors, distributed across 12 out of 13 different subgroups (S, C, D, F, I, E, M, B, K, H, G, J, and A). Only subgroup M, which exclusively contains bZIP72, was omitted from our matrices as it was not part of our GAL4 activation domain (AD) vector collection. These analyses confirmed the interaction between FT and FD, and TFL1 and FD (Fig. 7A; Supplementary Table S6). Furthermore, nine strong and two

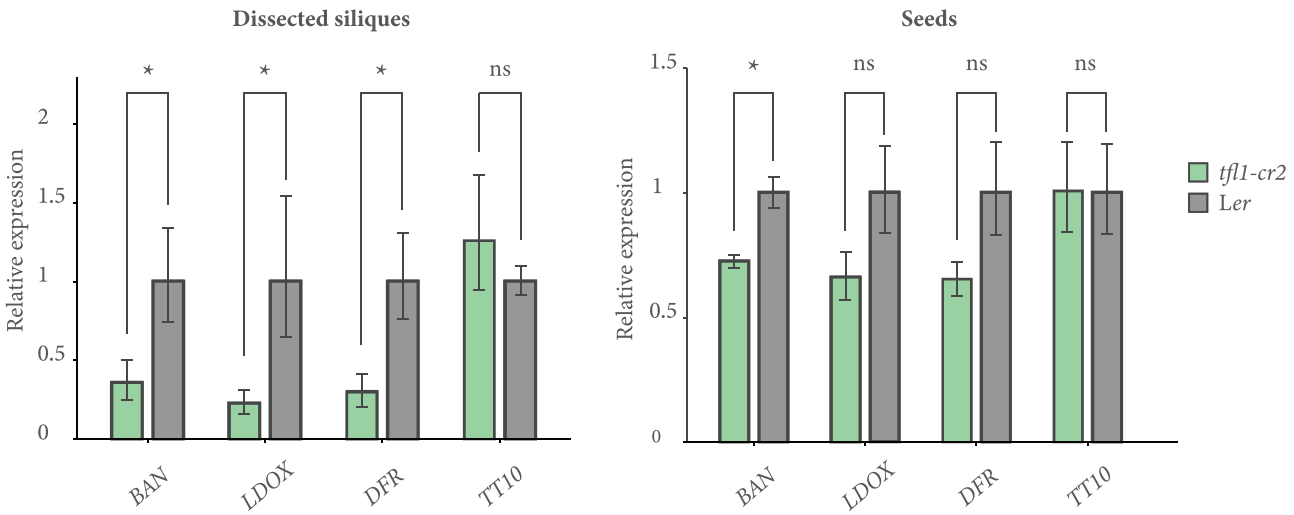

Fig. 6. Expression analysis of a subset of proanthocyanidin biosynthesis genes in *tfl1-cr2* mutants. Real-time PCR of dissected siliques (left) and seeds (right) at the torpedo stage of development from wild-type L*er* and *tfl1-cr2* mutant plants grown at continuous 22 °C. Data represents the mean and SE of three biological replicates. Asterisks indicate statistically significant differences compared with the wild-type L*er* using a Student's *t*-test. *$P<0.05$.

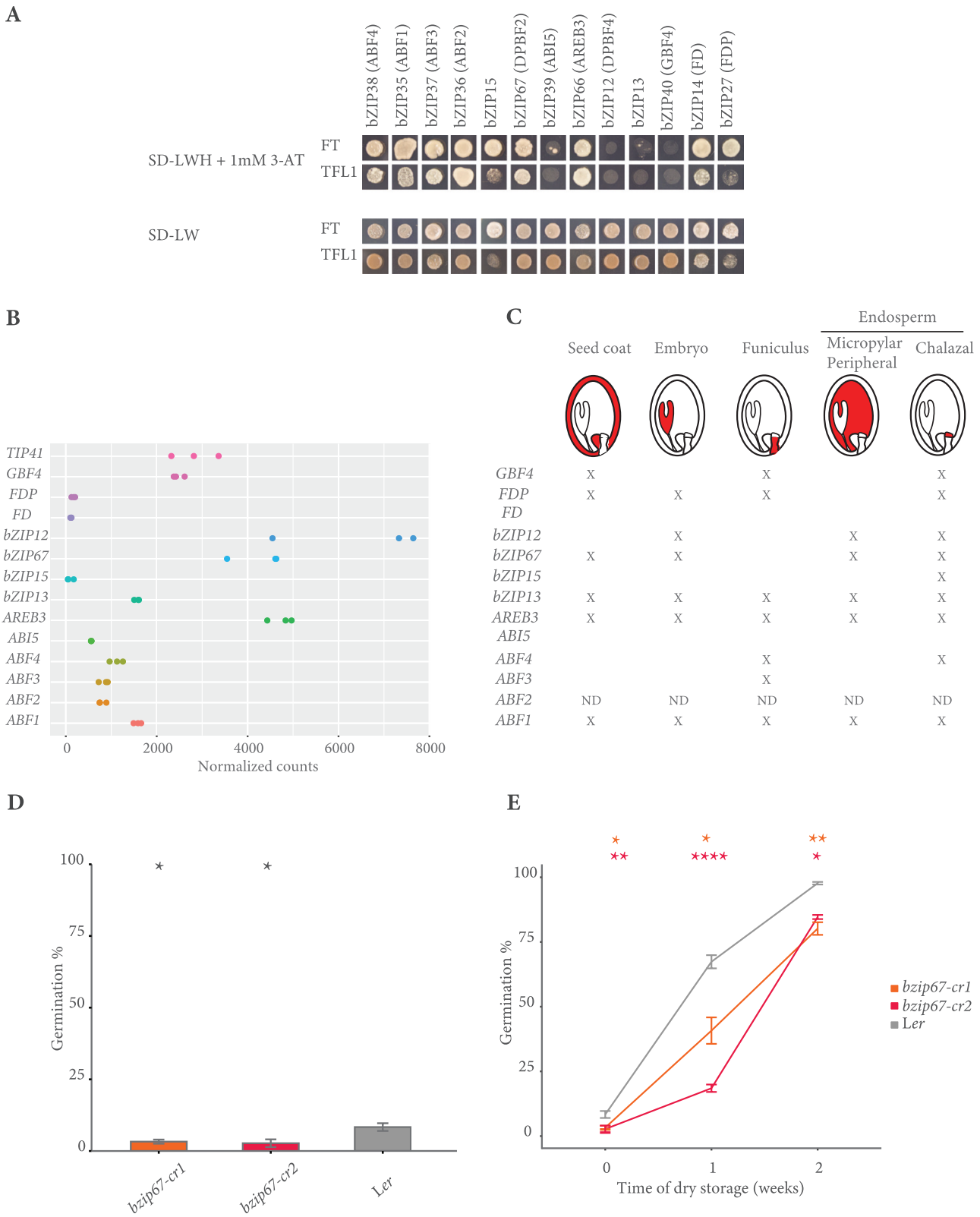

Fig. 7. bZIP subgroup A members as potential mediators of FT and TFL1 functions in seeds. (A) Yeast two-hybrid assays showing the protein–protein interaction capacity of FT, TFL1, and the 13 members of the bZIP subgroup A. (B) Expression of the 13 members of the *bZIP* group A in seeds at the torpedo stage of embryo development, represented as normalized counts (based on RNAseq). The *TIP41* gene is included as a reference. (C) Presence–absence table of the 13 members of the *bZIP* group A in different seed-related compartments (based on the seed BAR eFP Browser). Seed

compartments are highlighted in red and include seed coat, embryo, funiculus, and endosperm (subdivided into micropylar and peripheral or chalazal). Presence is marked with an 'X'. ND: not determined. (D) Germination of freshly harvested *bzip67-cr* seeds from plants grown at continuous 22 °C scored 7 d after sowing. Dormancy is assessed by evaluating the germination percentage 7 d after sowing freshly harvested seeds. The lower the germination percentage, the higher the dormancy level. (E) Summary of germination results scored after several weeks of dry storage of *bzip67-cr* seeds from plants grown at continuous 22 °C. (D and E) Per genotype, four biological replicates that include seeds from five different plants were tested. Asterisks indicate statistically significant differences compared with the wild-type L*er* using a TukeyHSD test (D) and a Dunn test (E). ns (not significant); $P>0.05$; *$P<0.05$; **$P<0.01$; ***$P<0.001$, ****$P<0.0001$.

weaker additional interacting partners were identified for FT, along with seven strong and two weaker additional interacting partners for TFL1 (Fig. 7A; Supplementary Table S6). It is important to acknowledge, however, that interactions and interaction strengths identified through Y2H screens may not fully reflect the complexity and quantitative differences of *in vivo* interactions for PEBPs and bZIPs, necessitating further validation under physiological conditions. Remarkably, all identified *in vitro* interactors are part of the A-subgroup, and a substantial subset is shared between FT and TFL1 (Supplementary Table S6). Specifically, the bZIP members of the A-subgroup include several members acting at the core of abscisic acid (ABA) signaling. These have also been associated with regulating later phases of seed development and maturation (reviewed in Bensmihen *et al.*, 2005; Dröge-Laser *et al.*, 2018). For instance, *ABI5* and *DPBF4/EEL* regulate and fine-tune *Late Embryogenesis Abundant* (*LEA*) during the acquisition of seed desiccation tolerance (Bensmihen *et al.*, 2002). Additionally, some of the transcription factors within this subgroup play a role in modulating seed dormancy and germination, processes mediated by ABA. For example, *ABF3* and *ABI5* regulate ABA-mediated seed germination partially redundantly (Finkelstein *et al.*, 2005; Zhao *et al.*, 2020). To determine whether the 13 members of the bZIP subgroup A are expressed around the onset of seed maturation in Arabidopsis L*er*, and to assess their temporal overlap with *FT* and *TFL1* expression, we profiled gene expression in seeds at the torpedo stage of wild-type L*er* by RNAseq. Our analysis revealed that four members (*GBF4*, *bZIP12*, *bZIP67*, and *AREB3*) are highly expressed, six members (*bZIP13*, *ABI5*, and *ABF1–ABF4*) show moderate expression levels, and three members (*FD*, *FDP*, and *bZIP15*) exhibit low or hardly detectable expression levels (Fig. 7B).

Both *FT* and *TFL1* exhibit distinct tissue-specific expression patterns within the seed, with *FT* predominantly localized to maternal tissues, and *TFL1* also present in the chalazal endosperm (Fig. 3). To explore potential tissue-specific overlap between these PEBPs and the A-subgroup bZIP members, we employed publicly available gene expression data. Our analysis shows expression of various *bZIP* genes in maternal tissues (Fig. 7C). Combined with the yeast-based interaction data (Fig. 7A), this positions them as prime candidates for competitive interactions with FT and TFL1. Additionally, some *bZIP* genes show expression in the chalazal endosperm (Fig. 7C) and their encoded proteins are capable of interacting with TFL1 (Fig. 7A). These specific bZIPs could mediate effects on dormancy together with TFL1. Strikingly, of these proteins, bZIP67 has been previously associated with seed dormancy as an activator of *DELAY OF GERMINATION1* (*DOG1*) in Arabidopsis Col-0. DOG1 functions as a timer for seed dormancy release (Bryant *et al.*, 2019). Here, Arabidopsis L*er* is investigated, and therefore we generated *de novo* CRISPR/Cas9 mutants in this accession (Supplementary Fig. S6A, B). Phenotypic analysis showed a delayed germination in *bZIP67* loss-of-function mutants compared with wild-type L*er* (Fig. 7D, E).

Taking all of this into consideration, the results suggest that *FT* and *TFL1* exert an antagonistic role in the regulation of seed dormancy, probably partly mediated by their interaction with specific ABA-related bZIP proteins from the A-subgroup in different maternal or seed tissues, and by their impact on the expression of tannin biosynthesis genes in siliques.

Discussion

The *PEBP* family of genes, which encompasses *FT* and *TFL1*, is known to participate in the control of numerous signaling pathways governing growth and differentiation (Karlgren *et al.*, 2011). In particular, their central role in regulating meristem identity and flowering time is well established (Liu *et al.*, 2021). Nonetheless, a limited number of studies have suggested the potential involvement of *FT* and *TFL1* in modulating certain seed characteristics in Arabidopsis (Chen *et al.*, 2014; Zhang *et al.*, 2020). Here, we have characterized the role of *FT* and *TFL1* in Arabidopsis L*er* seeds and identified novel aspects of their functioning in various reproductive processes.

We found, for example, that the germination capacity of freshly harvested *tfl1* mutant seeds was greatly enhanced compared with the control (Fig. 1A, B). Conversely, the loss of *FT* function in the *ft* mutants significantly reduced this ability (Supplementary Fig. S3A, B), consistent with a previous report from Chen *et al.* (2014). Interestingly, wild-type dormancy levels were restored in the *ft tfl1* double mutant (Fig. 5A) and dormancy loss occurred at a similar rate to that in the wild type (Fig. 5B). These results reveal *TFL1* as a novel factor involved in the regulation of seed dormancy and suggest an opposite role for *FT* and *TFL1* in controlling this trait. Previous research has indicated that FT and TFL1 proteins act in opposite ways to mediate signals for floral transition (Kobayashi *et al.*, 1999; Zhu *et al.*, 2020). Within the SAM, these two proteins co-localize (Corbesier *et al.*, 2007; Goretti *et al.*, 2020), giving rise to a dynamic interplay primarily rooted in their competitive interactions for the chromatin-bound bZIP transcription factor FD at shared target loci (Zhu *et al.*, 2020). We present two distinct

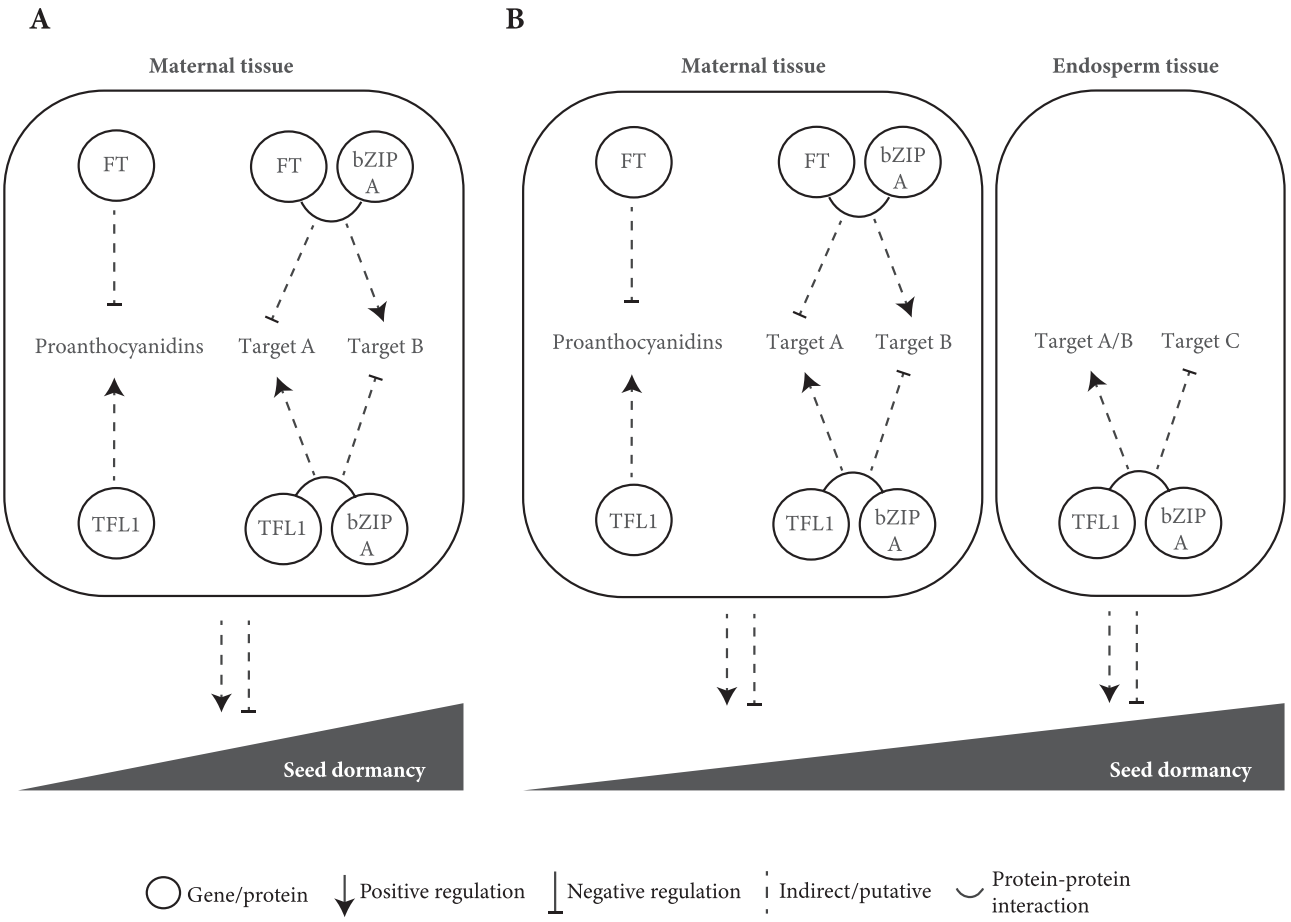

Fig. 8. Potential mechanisms underlying the contrasting roles of *FT* and *TFL1* in determining seed dormancy status. (A) Hypothesis 1 posits that both genes function within the same pathway, regulating proanthocyanidin biosynthesis in opposite ways and competing for interaction with bZIP members from subgroup A in maternal tissues, collectively influencing the final seed dormancy status. (B) Hypothesis 2 suggests that both genes operate partially within different pathways. In addition to its role in maternal tissues, TFL1 may also interact with other factors, including bZIP members from subgroup A in the endosperm, all contributing to the final seed dormancy status.

theories to explain the divergent function of *FT* and *TFL1* in determining the final seed dormancy status (Fig. 8). The first hypothesis postulates that these genes operate in the same pathway. This situation may be explained by the co-localization of the FT and TFL1 proteins within the Arabidopsis vascular bundles in the maternal tissue (Fig. 4; Supplementary Fig. S5B). Chen *et al.* (2014) proposed a hypothesis suggesting that FT exerts control over seed dormancy by modulating proanthocyanidin synthesis in siliques, followed by the transport of proanthocyanids to seeds and leading to subsequent alterations of tannin content in the seed coat. In an analogous experiment to that of Chen *et al.* (2014), we examined the expression level of genes responsible for proanthocyanidin synthesis in the siliques and seeds of a *tfl1-cr2* mutant. Our analysis unveiled a down-regulation of most of these genes in mutant siliques (Fig. 6). Notably, tannin biosynthesis in the seed coat during seed maturation plays a crucial role in establishing normal dormancy (Debeaujon *et al.*, 2000). Our expression results, demonstrating the down-regulation of tannin-related genes, align with the observed phenotype of *tfl1-cr2*, which exhibits a lack of dormancy. In addition to that, we have identified interactions involving FT, TFL1, and bZIP family subgroup A members (Fig. 7A; Supplementary Table S6). These interactions show that FT and TFL1 may control seed dormancy partly through an antagonistic mechanism mediated by bZIP proteins. For this mode of action, these proteins and interacting bZIPs must be co-localized in the same dormancy-determining tissues. Based on their interactions with both FT and TFL1, as well as their temporal and spatial expression patterns, *ABF1* and *AREB3* may serve as candidates (Figs 7B, C, 8A). These findings, collectively suggest the possibility that *TFL1* participates in the same regulatory pathway as *FT*, influencing seed dormancy through proanthocyanidin synthesis and engaging in competitive interactions for the same ABA-related bZIP proteins from the A-subgroup (Fig. 8A). The hypothesis that *FT* and *TFL1* control seed traits by acting through the same pathway and competing for the transcriptional regulation of the same target genes was also recently proposed by González-Suárez

et al. (2024). The exact nature and number of interactions potentially required for FT/TFL1-mediated seed control is unknown. However, similar to the redundant functions exhibited by multiple florigen-interacting bZIP transcription factors in flowering at the SAM (Martignago *et al.*, 2023), various FT/TFL1-interacting bZIP transcription factors could also have redundant or partially redundant roles in the regulation of seed dormancy.

Conversely, the second theory suggests that both genes function partly within different molecular pathways. This theoretical framework builds upon the first theory, which posits the co-localization of *FT* and *TFL1* in maternal vascular bundles and their function within the same pathway. Furthermore, it introduces an additional observation: the absence of detectable *FT* within the endosperm during the stages analyzed (Figs 3, 4), in contrast to the presence of the *TFL1* signal within this tissue (Fig. 3) (Zhang *et al.*, 2020). In the context of seed formation, the coordinated growth of the zygotic embryo, endosperm, and maternal seed coat plays a pivotal role in determining seed dormancy (Maia *et al.*, 2011). The noticeable variations in the spatial distribution of *FT* and *TFL1* within the silique and seeds could conceivably underlie their differential role in influencing dormancy. Building upon this second hypothesis, it is plausible that TFL1 also plays a role in controlling endosperm-directed dormancy. As an illustration, we showed that the *bzip67* mutant has a seed dormancy phenotype and that bZIP67 is expressed in the chalazal endosperm and codes for a protein that interacts with the endosperm-localized TFL1 protein. This might result in the targeting of distinct pathways, differing from those targeted by both FT and TFL1 in the maternal tissues (Fig. 8B).

Future research should include detailed analyses, such as protein pull-down assays of FT–GFP and TFL1–GFP transgenic lines followed by MS, to validate interactions with bZIP subgroup A members *in planta* or potentially uncover novel interactions. These studies will provide deeper insights into the underlying mechanisms by which *FT* and *TFL1* modulate seed traits such as dormancy.

In a study by Zhang *et al.* (2020), *TFL1* was identified as an important seed size regulator, influencing the rate of cellularization of the endosperm. Consistent with these findings, our *tfl1* mutants demonstrated a noticeable increase in both seed area and weight when compared with the wild-type L*er* (Fig. 2A, B). Although our analysis of single *ft* mutants did not show a consistently significant effect on seed mass and area (Figs 2, 5), the double *ft tfl1* mutants exhibited an intermediate seed area phenotype between that of *tfl1* and wild-type seeds. This suggests yet another contrasting role for *FT* and *TFL1* in controlling seed size. Our observation that *FT* is not detectably expressed in the endosperm indicates that this role might be indirect or through a different mechanism from that of *TFL1*. We hypothesize that the unloading of nutrients to the developing seed through the phloem of the funiculus, where *FT* is highly expressed, might exert an influence on seed development. The identification of genetic factors affecting seed traits is complicated by potential trade-offs between them. According to life-history theory, when limited resources are available for reproduction, there is typically a trade-off between fruit and seed number and size (Gnan *et al.*, 2014). In our experiments, *tfl1-cr2* and wild-type plants exhibited a number of seeds per silique comparable with that previously reported (Zhang *et al.*, 2020), while *tfl1-cr2* showed a reduced total seed yield per 10 plants (Fig. 5E, F). Conversely, under our growing conditions, both single *ft-cr3* and double *ft tfl1* mutants displayed a decrease in the number of seeds per silique (Fig. 5E). Yet, this decline did not affect total seed yield, which was increased compared with *tfl1-cr2* and the wild type (Fig. 5F), as was also previously shown in the Col-0 *ft-10* mutant (González-Suárez *et al.*, 2024). The presence of alterations in flowering time and inflorescence architecture in these mutants might be crucial for interpreting some of the phenotypic changes observed in the number of seeds per silique and total seed yield. In plant physiology, source–sink relationships refer to the balance between the production of photosynthates (source) in photosynthetic tissues such as leaves, and their utilization or storage (sink) in various organs, including the developing seed (Smith *et al.*, 2018). Based on this premise, we hypothesize that the observed changes in seed size and total number of seeds per plant might be attributed to shifts in sink–source dynamics resulting from disruptions of *FT* and *TFL1*. In other words, in a late-flowering *ft* mutant, an increased number of leaves and enhanced branching results in a greater abundance of source tissues. This surplus energy may be allocated to support the production of additional flowers and fruits, ultimately leading to a higher total seed yield. Conversely, in an early-flowering *tfl1* mutant, a reduced number of source tissues is present and the total number of siliques is reduced as well. Therefore, the energy may be dedicated to generating fewer seeds with increased size, thereby increasing vigor. A similar hypothesis was already formulated for *apetala2* (*ap2*) mutants, which also exhibit effects on flowering time, seed size, seed weight, and accumulation of seed reserves (Jofuku *et al.*, 2005; Ohto *et al.*, 2005). We hypothesize that a similar explanation underlies the apparently complex and partly contrasting results we achieved regarding the role of *FT* and *TFL1* in determining seed size and yield.

In summary, this study presents a comprehensive and detailed characterization of *FT* and *TFL1* in Arabidopsis L*er* seeds. Our findings shed light on previously unexplored and conserved facets of their contributions to seed vigor and overall seed yield, proposing *TFL1* as a newly identified regulator of seed dormancy. These genes might also play a role in other traits related to seed vigor. For instance, in 2020, a genome-wide analysis of the germination efficiency of Arabidopsis accessions after different accelerated seed aging methods identified *FT* within one of the putative genomic regions associated with variation in seed longevity (Renard *et al.*, 2020). Furthermore, a role for *FT* in the temperature-dependent control of fruit length, seed

number, and seed area was shown recently (González-Suárez *et al.*, 2024). Together, this highlights the complex and dynamic roles of *FT* and *TFL1* in fine-tuning seed quality characteristics and total seed yield, with the potential to unlock valuable insights that can shape the future of agriculture.

Supplementary data

The following supplementary data are available at *JXB* online.

Table S1. Primers used for the cloning of CRISPR/Cas9 constructs.

Table S2. Overview of all constructs engineered for this study.

Table S3. Primers used for the cloning of reporter lines.

Table S4. Primers used for plant genotyping.

Table S5. Primers used for RT-qPCR.

Table S6. Summary of results from the protein–protein interaction assays.

Fig. S1. DNA alignment of the various *ft* and *tfl1* mutants used in this study and their effect on flowering and plant architecture.

Fig. S2. Protein alignment of the various *FT* and *TFL1* mutants used in this study.

Fig. S3. Seed germination of different *ft* mutants.

Fig. S4. Design and localization in vegetative tissues of transcriptional *FT* and *TFL1* reporter lines.

Fig. S5. Design of translational *FT-GFP* and *TFL1-GFP* reporter lines, and localization of *FT-GFP* in developing seed.

Fig. S6. DNA and protein alignment of the various *bZIP67* mutants used in this study.

Acknowledgements

We thank Professor Leonie Bentsink for useful discussions and suggestions.

Author contributions

JNB, MF, GCA, and RGHI: conceptualization; LAJW: methodology; JNB and HN: formal analysis, JNB, FvW, and VW: investigation; HN: data curation; JNB: visualization and writing—original draft; JNB, LAJW, VW, GCA, and RGHI: writing—review and editing; MF, GCA, and RGHI: supervision; RGHI: funding acquisition.

Conflict of interest

The authors declare no conflict of interest.

Funding

This work was supported by the Dutch national funding agency Nederlandse Organisatie voor Wetenschappelijk Onderzoek (NWO), as part of the VICI project 'Climate Proof Plant Reproduction' (grant no. 16129).

Data availability

All raw data underlying the results presented in this study are available upon request.

The RNA-seq data underlying this article are available in the NCBI Sequence Read Archive at https://www.ncbi.nlm.nih.gov/bioproject/PRJNA1054800 or under the BioProject accession PRJNA1054800.

References

Ahn JH, Miller D, Winter VJ, Banfield MJ, Jeong HL, So YY, Henz SR, Brady RL, Weigel D. 2006. A divergent external loop confers antagonistic activity on floral regulators FT and TFL1. The EMBO Journal **25**, 605–614.

Alvarez J, Guli CL, Yu X-H, Smyth DR. 1992. Terminal flower: a gene affecting inflorescence development in *Arabidopsis thaliana*. The Plant Journal **2**, 103–116.

Attuluri VPS, Sánchez López JF, Maier L, Paruch K, Robert HS. 2022. Comparing the efficiency of six clearing methods in developing seeds of *Arabidopsis thaliana*. Plant Reproduction **35**, 279–293.

Benlloch R, Berbel A, Serrano-Mislata A, Madueño F. 2007. Floral initiation and inflorescence architecture: a comparative view. Annals of Botany **100**, 659–676.

Bensmihen S, Giraudat J, Parcy F. 2005. Characterization of three homologous basic leucine zipper transcription factors (bZIP) of the ABI5 family during *Arabidopsis thaliana* embryo maturation. Journal of Experimental Botany **56**, 597–603.

Bensmihen S, Rippa S, Lambert G, Jublot D, Pautot V, Granier F, Giraudat J, Parcy F. 2002. The homologous ABI5 and EEL transcription factors function antagonistically to fine-tune gene expression during late embryogenesis. The Plant Cell **14**, 1391–1403.

Bolger AM, Lohse M, Usadel B. 2014. Trimmomatic: a flexible trimmer for Illumina sequence data. Bioinformatics **30**, 2114–2120.

Bradley D, Ratcliffe O, Vincent C, Carpenter R, Coen E. 1997. Inflorescence commitment and architecture in Arabidopsis. Science **275**, 80–83.

Bryant FM, Hughes D, Hassani-Pak K, Eastmond PJ. 2019. Basic LEUCINE ZIPPER TRANSCRIPTION FACTOR67 transactivates DELAY OF GERMINATION1 to establish primary seed dormancy in Arabidopsis. The Plant Cell **31**, 1276–1288.

Chen F, Li Y, Li X, Li W, Xu J, Cao H, Wang Z, Li Y, Soppe WJJ, Liu Y. 2021. Ectopic expression of the Arabidopsis florigen gene FLOWERING LOCUS T in seeds enhances seed dormancy via the GA and DOG1 pathways. The Plant Journal **107**, 909–924.

Chen M, MacGregor DR, Dave A, Florance H, Moore K, Paszkiewicz K, Smirnoff N, Graham IA, Penfield S. 2014. Maternal temperature history activates Flowering Locus T in fruits to control progeny dormancy according to time of year. Proceedings of the National Academy of Sciences, USA **111**, 18787–18792.

Chen M, Penfield S. 2018. Feedback regulation of COOLAIR expression controls seed dormancy and flowering time. Science **360**, 1014–1017.

Conant D, Hsiau T, Rossi N, *et al*. 2022. Inference of CRISPR edits from Sanger trace data. The CRISPR Journal **5**, 123–130.

Concordet JP, Haeussler M. 2018. CRISPOR: intuitive guide selection for CRISPR/Cas9 genome editing experiments and screens. Nucleic Acids Research **46**, W242–W245.

Conti L, Bradley D. 2007. TERMINAL FLOWER1 is a mobile signal controlling Arabidopsis architecture. The Plant Cell **19**, 767–778.

Corbesier L, Vincent C, Jang S, *et al*. 2007. FT protein movement contributes to long-distance signaling in floral induction of Arabidopsis. Science **316**, 1030–1033.

Czechowski T, Stitt M, Altmann T, Udvardi MK, Scheible WR. 2005. Genome-wide identification and testing of superior reference genes for transcript normalization in Arabidopsis. Plant Physiology **139**, 5–17.

Debeaujon I, Léon-Kloosterziel KM, Koornneef M. 2000. Influence of the testa on seed dormancy, germination, and longevity in Arabidopsis. Plant Physiology **122**, 403–414.

Debeaujon I, Nesi N, Perez P, Devic M, Grandjean O, Caboche M, Lepiniec L. 2003. Proanthocyanidin-accumulating cells in Arabidopsis testa: regulation of differentiation and role in seed development. The Plant Cell **15**, 2514–2531.

de Folter S, Immink RGH. 2011. Yeast protein–protein interaction assays and screens. Methods in Molecular Biology **754**, 145–165.

dos Reis Moreira J, Quiñones A, Lira BS, *et al*. 2022. SELF PRUNING 3C is a flowering repressor that modulates seed germination, root architecture, and drought responses. Journal of Experimental Botany **73**, 6226–6240.

Dröge-Laser W, Snoek BL, Snel B, Weiste C. 2018. The Arabidopsis bZIP transcription factor family—an update. Current Opinion in Plant Biology **45**, 36–49.

Finkelstein R, Gampala SS, Lynch TJ, Thomas TL, Rock CD. 2005. Redundant and distinct functions of the ABA response loci ABA-INSENSITIVE (ABI) 5 and ABRE-BINDING FACTOR (ABF) 3. Plant Molecular Biology **59**, 253–267.

Gnan S, Priest A, Kover PX. 2014. The genetic basis of natural variation in seed size and seed number and their trade-off using *Arabidopsis thaliana* MAGIC lines. Genetics **198**, 1751–1758.

González-Suárez P, Walker CH, Lock T, Bennett T. 2024. FLOWERING LOCUS T-mediated thermal signalling regulates age-dependent inflorescence development in *Arabidopsis thaliana*. Journal of Experimental Botany **75**, 4400–4414.

Goretti D, Silvestre M, Collani S, Langenecker T, Méndez C, Madueño F, Schmid M. 2020. TERMINAL FLOWER1 functions as a mobile transcriptional cofactor in the shoot apical meristem. Plant Physiology **182**, 2081–2095.

Guo Z, Dzinyela R, Yang L, Hwarari D. 2024. bZIP transcription factors: structure, modification, abiotic stress responses and application in plant improvement. Plants **13**, 2058.

He Y, Li L, Shi W, Tan J, Luo X, Zheng S, Chen W, Li J, Zhuang C, Jiang D. 2022. Florigen repression complexes involving rice CENTRORADIALIS2 regulate grain size. Plant Physiology **190**, 1260–1274.

Holdsworth MJ, Bentsink L, Soppe WJJ. 2008. Molecular networks regulating Arabidopsis seed maturation, after-ripening, dormancy and germination. New Phytologist **179**, 33–54.

Jack T. 2004. Molecular and genetic mechanisms of floral control. The Plant Cell **16**, S1–S17.

Jofuku KD, Omidyar PK, Gee Z, Okamuro JK. 2005. Control of seed mass and seed yield by the floral homeotic gene APETALA2. Proceedings of the National Academy of Sciences, USA **102**, 3117–3122.

Joosen RVL, Kodde J, Willems LAJ, Ligterink W, Van Der Plas LHW, Hilhorst HWM. 2010. Germinator: a software package for high-throughput scoring and curve fitting of Arabidopsis seed germination. The Plant Journal **62**, 148–159.

Kardailsky I, Shukla VK, Ahn JH, Dagenais N, Christensen SK, Nguyen JT, Chory J, Harrison MJ, Weigel D. 1999. Activation tagging of the floral inducer FT. Science **286**, 1962–1965.

Karlgren A, Gyllenstrand N, Källman T, Sundström JF, Moore D, Lascoux M, Lagercrantz U. 2011. Evolution of the PEBP gene family in plants: functional diversification in seed plant evolution. Plant Physiology **156**, 1967–1977.

Kim D, Paggi JM, Park C, Bennett C, Salzberg SL. 2019. Graph-based genome alignment and genotyping with HISAT2 and HISAT-genotype. Nature Biotechnology **37**, 907–915.

Kobayashi Y, Kaya H, Goto K, Iwabuchi M, Araki T. 1999. A pair of related genes with antagonistic roles in mediating flowering signals. Science **286**, 1960–1962.

Koornneef M, Alonso-Blanco C, Bentsink L, Blankestijn-de Vries H, Debeaujon I, Hanhart CJ, León-Kloosterziel KM, Peeters AJM, Raz V. 2000. The genetics of seed dormancy in *Arabidopsis thaliana*. In: Viémont JD, Crabbé J, eds. Dormancy in plants: from whole plant behaviour to cellular control. Wallingford, UK: CABI Publishing, 365–373.

Koornneef M, Alonso-Blanco C, Blankestijn-De Vries H, Hanhart CJ, Peeters AJM. 1998. Genetic interactions among late-flowering mutants of Arabidopsis. Genetics **148**, 885–892.

Kurihara D, Mizuta Y, Nagahara S, Higashiyama T. 2021. ClearSeeAlpha: advanced optical clearing for whole-plant imaging. Plant and Cell Physiology **62**, 1302–1310.

Leijten W, Koes R, Roobeek I, Frugis G. 2018. Translating flowering time from *Arabidopsis thaliana* to Brassicaceae and Asteraceae crop species. Plants **7**, 111.

Liu H, Ding Y, Zhou Y, Jin W, Xie K, Chen LL. 2017. CRISPR-P 2.0: an improved CRISPR-Cas9 tool for genome editing in plants. Molecular Plant **10**, 530–532.

Liu L, Xuan L, Jiang Y, Yu H. 2021. Regulation by FLOWERING LOCUS T and TERMINAL FLOWER 1 in flowering time and plant architecture. Small Structures **2**.

Livak KJ, Schmittgen TD. 2001. Analysis of relative gene expression data using real-time quantitative PCR and the 2-ΔΔCT method. Methods **25**, 402–408.

Love MI, Huber W, Anders S. 2014. Moderated estimation of fold change and dispersion for RNAseq data with DESeq2. Genome Biology **15**, 550.

Maia J, Dekkers BJW, Provart NJ, Ligterink W, Hilhorst HWM. 2011. The re-establishment of desiccation tolerance in germinated *Arabidopsis thaliana* seeds and its associated transcriptome. PLoS One **6**, e29123.

Martignago D, da Silveira Falavigna V, Lombardi A, Gao H, Korwin Kurkowski P, Galbiati M, Conti L. 2023. The bZIP transcription factor AREB3 mediates FT signalling and floral transition at the Arabidopsis shoot apical meristem. PLoS Genetics **19**, e1010766.

Mathieu J, Warthmann N, Küttner F, Schmid M. 2007. Export of FT protein from phloem companion cells is sufficient for floral induction in Arabidopsis. Current Biology **17**, 1055–1060.

Moles AT, Ackerly DD, Webb CO, Tweddle JC, Dickie JB, Westoby M. 2005. A brief history of seed size. Science **307**, 576–580.

Moraes TS, Dornelas MC, Martinelli AP. 2019. FT/TFL1: calibrating plant architecture. Frontiers in Plant Science **10**, 97.

Ohto MA, Fischer RL, Goldberg RB, Nakamura K, Harada JJ. 2005. Control of seed mass by APETALA2. Proceedings of the National Academy of Sciences, USA **102**, 3123–3128.

Pertea M, Pertea GM, Antonescu CM, Chang T-C, Mendell JT, Salzberg SL. 2015. StringTie enables improved reconstruction of a transcriptome from RNA-seq reads. Nature Biotechnology **33**, 290–295.

Pruneda-Paz JL, Breton G, Nagel DH, Kang SE, Bonaldi K, Doherty CJ, Ravelo S, Galli M, Ecker JR, Kay SA. 2014. A genome-scale resource for the functional characterization of Arabidopsis transcription factors. Cell Reports **8**, 622–632.

Ratcliffe OJ, Bradley DJ, Coen ES. 1999. Separation of shoot and floral identity in Arabidopsis. Development **126**, 1109–1120.

Reed RC, Bradford KJ, Khanday I. 2022. Seed germination and vigor: ensuring crop sustainability in a changing climate. Heredity **128**, 450–459.

Renard J, Niñoles R, Martínez-Almonacid I, Gayubas B, Mateos-Fernández R, Bissoli G, Bueso E, Serrano R, Gadea J. 2020. Identification of novel seed longevity genes related to oxidative stress and seed coat by genome-wide association studies and reverse genetics. Plant, Cell & Environment **43**, 2523–2539.

Robles P, Pelaz S. 2005. Flower and fruit development in *Arabidopsis thaliana*. International Journal of Developmental Biology **49**, 633–643.

Shannon S, Ry Meeks-Wagner D. 1991. A mutation in the Arabidopsis TFL1 gene affects inflorescence meristem development. The Plant Cell **3**, 877–892.

Simon R, Igeño MI, Coupland G. 1996. Activation of floral meristem identity genes in Arabidopsis. Nature **384**, 59–62.

Smith MR, Rao IM, Merchant A. 2018. Source–sink relationships in crop plants and their influence on yield development and nutritional quality. Frontiers in Plant Science **9**, 1889.

Song J, Sun S, Ren H, Grison M, Boutté Y, Bai W, Men S. 2019. The SmO1 family of sterol 4α-methyl oxidases is essential for auxin- and cytokinin-regulated embryogenesis. Plant Physiology **181**, 578–594.

Takada S, Goto K. 2003. TERMINAL FLOWER2, an Arabidopsis homolog of HETEROCHROMATIN PROTEIN1, counteracts the activation of FLOWERING LOCUS T by CONSTANS in the vascular tissues of leaves to regulate flowering time. The Plant Cell **15**, 2856–2865.

Verma S, Attuluri VPS, Robert HS. 2022. Transcriptional control of Arabidopsis seed development. Planta **255**, 90.

Wang S, Yang Y, Chen F, Jiang J. 2022. Functional diversification and molecular mechanisms of FLOWERING LOCUS T/TERMINAL FLOWER 1 family genes in horticultural plants. Molecular Horticulture **2**, 19.

Weber E, Engler C, Gruetzner R, Werner S, Marillonnet S. 2011. A modular cloning system for standardized assembly of multigene constructs. PLoS One **6**, e16765.

Wickland DP, Hanzawa Y. 2015. The FLOWERING LOCUS T/TERMINAL FLOWER 1 gene family: functional evolution and molecular mechanisms. Molecular Plant **8**, 983–997.

Wigge PA. 2011. FT, a mobile developmental signal in plants. Current Biology **21**, R374–R378.

Willemsen V, Wolkenfelt H, de Vrieze G, Weisbeek P, Scheres B. 1998. The HOBBIT gene is required for formation of the root meristem in the Arabidopsis embryo. Development **125**, 521–531.

Yang Z, Chen L, Kohnen MV, *et al*. 2019. Identification and characterization of the PEBP family genes in Moso bo (*Phyllostachys heterocycla*). Scientific Reports **9**, 14998.

Zhang B, Li C, Li Y, Yu H. 2020. Mobile TERMINAL FLOWER1 determines seed size in Arabidopsis. Nature Plants **6**, 1146–1157.

Zhao H, Nie K, Zhou H, Yan X, Zhan Q, Zheng Y, Song C-P. 2020. ABI5 modulates seed germination via feedback regulation of the expression of the PYR/PYL/RCAR ABA receptor genes. New Phytologist **228**, 596–608.

Zhou L, Dresselhaus T. 2019. Friend or foe: signaling mechanisms during double fertilization in flowering seed plants. Current Topics in Developmental Biology **131**, 453–496.

Zhu Y, Klasfeld S, Jeong CW, Jin R, Goto K, Yamaguchi N, Wagner D. 2020. TERMINAL FLOWER 1–FD complex target genes and competition with FLOWERING LOCUS T. Nature Communications **11**, 5118.